The Self-Heating of Sulphide Mixtures

Rebecca Payant

Department of Mining and Materials Engineering
McGill University
Montreal, Canada

August 2010

A thesis submitted to McGill University
in partial fulfilment of the requirements of the degree of
Master of Engineering

Abstract

Under certain conditions of moisture and oxygen, sulphides can spontaneously heat, known as self-heating or pyrophoric behaviour. In this thesis the hypothesis that galvanic interaction between some sulphides can promote self-heating is tested. Galvanic interaction is controlled by rest-potential difference between the minerals and the surface area of contact (particle size). In order of decreasing rest-potential, four sulphides were tested: pyrite, chalcopyrite, sphalerite and galena. Two series of samples consisting of mixtures of two sulphides each representing a mass fraction of 50 % were run in standard self-heating tests. The first series comprised five mixtures were prepared, two with low rest-potential difference (pyrite-chalcopyrite and chalcopyrite-sphalerite) and three with high rest-potential difference (pyrite-galena, chalcopyrite-galena and pyrite-sphalerite). The second series was performed on a pyrite-sphalerite mixture at four particle sizes (80 % passing 850 μm, 300 μm, 75 μm and 38 μm). The first series showed that the individual sulphides and the mixtures of low rest-potential difference did not self-heat but the mixtures of high rest-potential difference did self-heat. The second series showed that self-heating increased inversely with particle size (increasing specific surface area) and that it was the fineness of the pyrite (the high rest-potential sulphide) that governed the self-heating effect, indicating the rate-limiting reaction is reduction at the more noble pyrite (cathodic mineral). The increase in self-heating with high rest-potential difference and increasing particle fineness supports the hypothesis that galvanic interaction contributes significantly to sulphide self-heating. A possible mechanism based on the H_2S hypothesis is proposed. The understanding gained will be of interest to those involved in storage, shipping and disposal of sulphide mineral mixtures.

Résumé

Sous certaines conditions d'air et d'humidité, les sulfures peuvent s'auto-échauffer, et dans un cas extrême, subir une auto-combustion. Le présent mémoire étudie l'hypothèse qu'un effet galvanique entre certains sulfures pourrait promouvoir l'auto-échauffement. L'effet galvanique est contrôlé par la différence de potentiel de corrosion (ΔE) et l'aire de surface en contact (granulométrie). En ordre décroissant de potentiel de corrosion, les quatre sulfures étudiés sont: la pyrite, la chalcopyrite, le sulfure de zinc et la galène. Deux séries d'échantillons ont été soumises à des tests standards d'auto-échauffement. Les séries se composaient de mélanges de deux sulfures, chaque sulfure représentant une fraction massique de 50 %. Dans la première série, cinq mélanges ont été préparés, deux avec une différence de potentiel de corrosion de 0,1 volt (pyrite-chalcopyrite et chalcopyrite-sulfure de zinc) et trois d'un potentiel de corrosion > 0,2 volt (pyrite-galène, chalcopyrite-galène et pyrite-sulfure de zinc). Dans la deuxième série, un mélange de pyrite-sulfure de zinc à quatre granulométries différentes (80 % passant 850 µm, 300 µm, 75 µm et 38 µm) a été étudié. Dans la première série, les sulfures individuels et les mélanges possédant une différence de potentiel de corrosion de 0,1 volt ne se sont pas auto-échauffés, mais les mélanges ayant une différence de potentiel de corrosion de > 0,2 volt se sont auto-échauffés. La deuxième série étudiée montre que l'auto-échauffement augmente de façon inversement proportionnelle à la grosseur des particules (aire de contact plus grande) et que la finesse de la pyrite (sulfure au potentiel de corrosion le plus élevé) gouverne l'effet galvanique, indiquant que la réaction cinétiquement limitante est la réduction sur le sulfure le plus noble, donc la pyrite (la cathode). L'augmentation d'auto-échauffement dû à la différence de potentiel de corrosion > 0,2 volt et une granulométrie fine mettent en évidence l'hypothèse qu'un effet galvanique contribue d'une façon significative à l'auto-échauffement des sulfures. Un mécanisme basé sur l'hypothèse de l'acide sulfhydrique (H_2S) est suggéré. Les résultats seront d'intérêt pour les personnes responsables de l'entreposage, du transport et de l'élimination de mélanges de sulfure.

Acknowledgements

I would like to take this opportunity to thank all the people that have helped this project come to life;

To Professor James A. Finch, thank you for giving me this opportunity, providing constant encouragement, motivation, new ideas and input to my work.

Many thanks to Mr. Frank Rosenblum and Dr. Stéphanie Somot for their dedication to the project, all the training, their ideas and patience, to Dr. S. Ramachandra Rao and Mr. Jan Nesset for ideas and good discussions.

A big thank you to Mr. Ray Langlois for constant technical support, jokes and patience, as well as Ms. Monique Riendeau for technical support.

Thanks to Mr. Edwin van Der Spuy, for helping put this thesis together and to Professor George P. Demopoulos.

Thank you to CAMIRO MPD (representing Vale, Teck, Xstrata Zinc, Xstrata Process Support, Golder Associates, and Cytec), NSERC (Natural Sciences and Engineering Research Council of Canada) and for financial support under the NSERC CRD (Collaborative Research and Development) program and Xstrata Nickel for supplying samples.

To the members of the McGill Mineral Processing Group (2007-2010) for help and good times.

Finally, I would like to thank all of my family and friends for their constant support and encouragement.

Table of Contents

List of Figures

List of Tables

Chapter 1 Introduction

1.1. Sulphide Self-Heating

Sulphide mineral ores have been mined for more than a century as the major source of most base metals such as copper, zinc, nickel and lead. Once the ore is extracted, the sulphide minerals are liberated by size reduction (crushing and grinding), concentrated by flotation, and the concentrates sent for the further processing to extract the metal (smelting and refining). At the various stages from mining to concentrate shipping and tailings storage the sulphides are exposed to a variety of environments, which under certain conditions of air humidity and temperature can cause them to heat. Since no external heat source is involved, this pyrophoric process is known as spontaneous heating or, more commonly, self-heating. The self-heating of sulphides is associated with oxidation reactions under moist conditions. If the heat generated is greater than the heat dissipated, the sulphides will self-heat. This can make working conditions potentially dangerous as oxygen is consumed from the surrounding air and significant quantities of sulphur dioxide (SO_2) can be released (Ninteman, 1978).

If uncontrolled, ignition can occur which is particularly difficult to control. In 1914, the Pocahontas operation in the Joplin district of Missouri was abandoned due to self-heating attributed to marcasite (a form of iron sulphide, FeS_2) that caused fires to spread throughout the mine. Mount Isa Mine Ltd. in Australia has been documented for cases of spontaneous oxidation and combustion of sulphides in underground mines (Ninteman, 1978). At the Sullivan Mine, Kimberley, British Colombia ore high in iron sulphides was left unattended underground for several days. It began to heat to the point of smouldering red. Temperatures were said to have reached higher than 500 °C (O'Brien and Banks, 1926). A section of the mine was closed as a consequence. The Sullivan fire made the front cover of the CIM Bulletin in November 1977 (Figure 1.1), indicating the long-standing nature of the problem. Brunswick Mine developed an underground fire due to back-filling with iron sulphide-rich tailings. The fire required venting and lasted

some 25 years (Noranda Technology Centre, 1975). The problem of sulphide self-heating clearly has economic as well as environmental impacts (Ninteman, 1978).

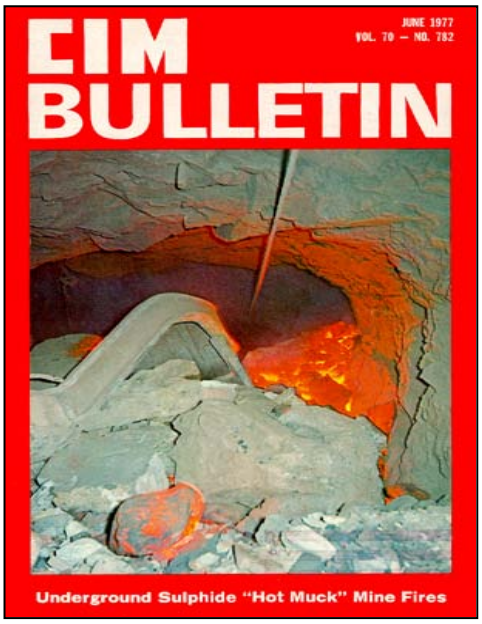

Figure 1.1: Underground sulphide mine fire at Kimberly, BC, 1977. Cover of the June 1977 issue of CIM Bulletin. Reprinted with permission of the Canadian Institute of Mining, Metallurgy and Petroleum

In some cases, self-heating of sulphides has led to loss of life. Among the earliest records is a case in 1862 when a Chilean ship carrying copper ore caught fire (Kirshenbaum, 1968). The spontaneous combustion of copper concentrates carried by the N.Y.K. liner s/s "Bokayo Muru" was said to be the reason for it sinking (Ninteman, 1978). In 1916, 163 men were killed in the granite mountain shaft in Butte, Montana. Almost thirty years later, in 1945, 355 lives were taken by fire at the Braden mine in Chile. In 1972, spontaneous combustion was attributed to the death of 91 miners at the Sunshine Mine in Idaho. More recently, in 1986 a fire in Wilberg Collierg, Utah cost of 26 lives (Stachulak, 1990).

Iron sulphides are the minerals most associated with self-heating (Rosenblum and Spira, 1995). Pyrrhotite, in particular, has been studied extensively in recognition of its known rapid oxidation leading to a fast self-heating response. The majority of other sulphides, alone at least, are not prone to self-heating. This situation may

change when mixtures of sulphides are formed. It has been noted that when some sulphides are mixed with pyrite they can oxidize at a much faster rate (Klassen and Mokrousov, 1963). In several cases of self-heating, researchers have suspected that electrochemical (electron transfer) reactions are involved (Kirshenbaum, 1968; Ninteman, 1978; Rosenblum and Spira, 1995; Wang, 2007). A common electrochemical reaction between contacting sulphide minerals in the presence of moisture is galvanic interaction (Rao and Leja, 2004). This forms the focus of the thesis.

1.2. Objective

The objective is to determine the possible role of galvanic effects in self-heating by testing sulphide mixtures of controlled rest-potential difference and particle size.

1.3. Thesis Organization

The thesis consists of six chapters. Chapter 1 is the Introduction to the topic and the thesis objective. Chapter 2 is the Literature Review, which provides the background. Chapter 3 is the Experimental Procedure where materials and methods are explained. The results obtained are presented in Chapter 4 and discussed in Chapter 5. Finally, Chapter 6 is the Conclusions and Recommendations. Literature Review.

Chapter 2 Literature Review

2.1. Methods to Evaluate Self-Heating

Good (1977) performed combustion tests for Cominco at the Sullivan Mine in Kimberley, BC. An apparatus was designed to test the ignition temperature of samples of particle size -200 mesh (-74 μm) in an oxygen atmosphere (Figure 2.1). The temperature and sulphur dioxide release were monitored up to the ignition point. Typical heating and sulphur dioxide emission curves are presented in Figure 2.2. Large amounts of sulphur dioxide were released a few minutes into the test and again once the ignition point was reached. The ignition temperatures ranged from 205-515 °C with most samples falling within 385-450 °C.

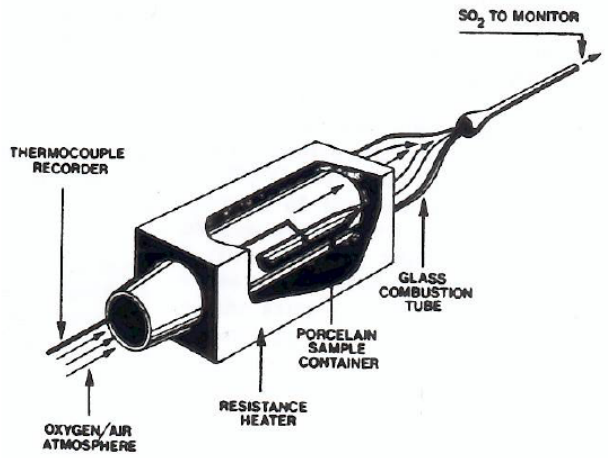

Figure 2.1: Combustion test apparatus (Good, 1977). Reprinted with permission of the Canadian Institute of Mining, Metallurgy and Petroleum

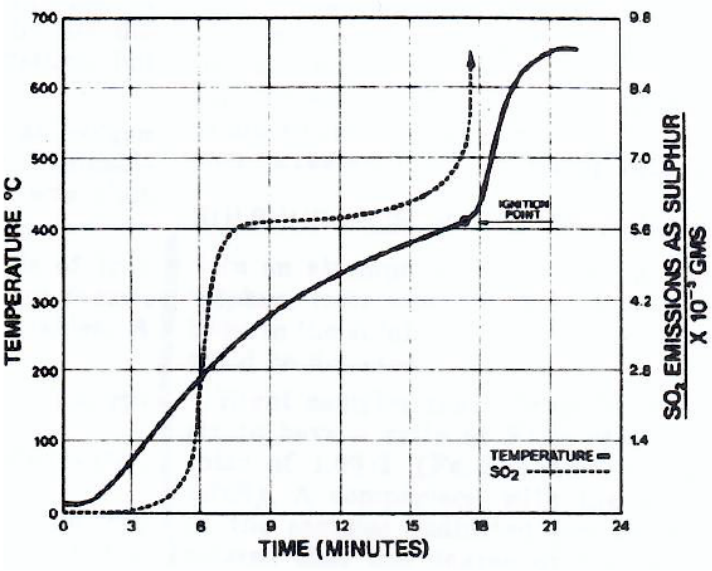

Figure 2.2: Typical heating curve and SO_2 emissions (Good, 1977). Reprinted with permission of the Canadian Institute of Mining, Metallurgy and Petroleum

The West German Office of Material Testing (BAM) developed a method to determine the self-heating properties of sulphide materials. Samples of 3200 cm^3 volume were placed in an oven at 200 °C for 48 hours. A thermocouple embedded in the sample measured the sample temperature against time. A sample was considered spontaneously combustible (self-igniting) if its temperature rose above 500 °C within the 48-hour period. A series of 27 samples of lead, copper and zinc concentrates along with one pyrite concentrate was tested using this system. Little to no heating was observed for any of the samples (Wegener and Schlieper, 1977).

Meng et al. (1993) designed experiments to test the following: rate of oxygen depletion (absorption), initial self-heating temperature, self-heating rate and ignition temperature. The first set of tests measured the rate of oxygen absorption for a given mass of sulphide. A sample was placed in a sealed container of a known volume (i.e., known amount of air). Equation 2.1 was used to determine the rate of oxygen absorption (R_o) in $\frac{mL}{kg \cdot s}$.

$$R_o = \left(\frac{Q}{M \cdot t} \right) (C_o - C_i) \qquad (2.1)$$

where M is the mass of the sulphide in kg, Q is the volume of the container in mL, C_o and C_i are the initial and instantaneous concentration of oxygen in the container (%) and t is the time in seconds. The researchers considered that the greater the R_o the more reactive the sample.

A second set of tests measured the initial self-heating temperature and self-heating rate. A sulphide sample was placed in a container at a constant temperature and moisture of mass fraction 5 %. Air was continuously fed into the container and heat generated by the sample was measured by a thermocouple (Meng et al., 1993).

A third set of tests determined the ignition point of sulphide samples. To a given mass of sample, heated at a given rate, a small amount of oxygen was continuously added. As the sample begins to spontaneously heat, the temperature of the sample rises above that of the furnace. The intersection of sample and furnace temperature was taken as the ignition temperature (Meng et al., 1993).

In the 1990s a procedure known as fault tree analysis (FTA) was used to determine the inherent self-heating potential of sulphides and the optimal pathway for controlling self-heating. This technique expresses the cause and effect of self-heating in graphical form. It was based on the investigation of self-heating from more than 10 mines and an extensive review of the literature (Wu, 1995).

Wu and Li (2005) measured weight gain and oxygen absorption of sulphide samples using similar procedures to Meng et al. (1993). Samples were kept in a humidity chamber for 4-10 days, weighed daily and the sulphate and water-soluble iron content were determined. They found a positive linear trend between

the weight gain and oxygen absorption (Wu and Li, 2005). However, while the positive trend indicates the reactivity of the sample, it is not necessarily an accurate method to predict self-heating as later work showed that the rate of oxidation is not equivalent to self-heating (Wang, 2007; Wang et al., 2009). No relationship with sulphate content or water-soluble iron was observed.

The United Nations (U.N.) Recommendations on Transport of Dangerous Goods suggest there are two types of spontaneously combustible materials (United Nations, 2010). The first type is pyrophoric which ignites within 5 minutes of exposure to air and the second type refers to bulk samples that heat when exposed to air after hours or days. Sulphides fall into the second category.

The U.N. test employs a so-called basket method. Samples are in powder or granular form and a volume of 100 mm^3 is held in an open-top basket made of stainless steel net (mesh opening 0.05 mm) which is placed in an oven. The temperature of the sample and oven are recorded simultaneously with two thermocouples, one placed in the centre of the sample the other between the sample container and the oven wall. Testing begins at 140 °C for 24 hours. A positive result for spontaneous combustion is considered when the sample temperature rises 60 °C above that of the oven. If a negative result is obtained no further testing is done. If positive this leads to a second test in which the sample volume is reduced to 25 mm^3 and the sample is tested again at a temperature of 140 °C for 24 hours. A positive result from this second test sees the sample assigned to group II, substances which present some danger. A negative result places the material in group III, in which the substance presents low danger (United Nations, 2008; United Nations, 2010). A flow sheet showing the test methodology is presented in Figure 2.3. The U.N. regulations and requirements are also currently used by the U.S. Department of Transportation (DOT) and Transport Canada.

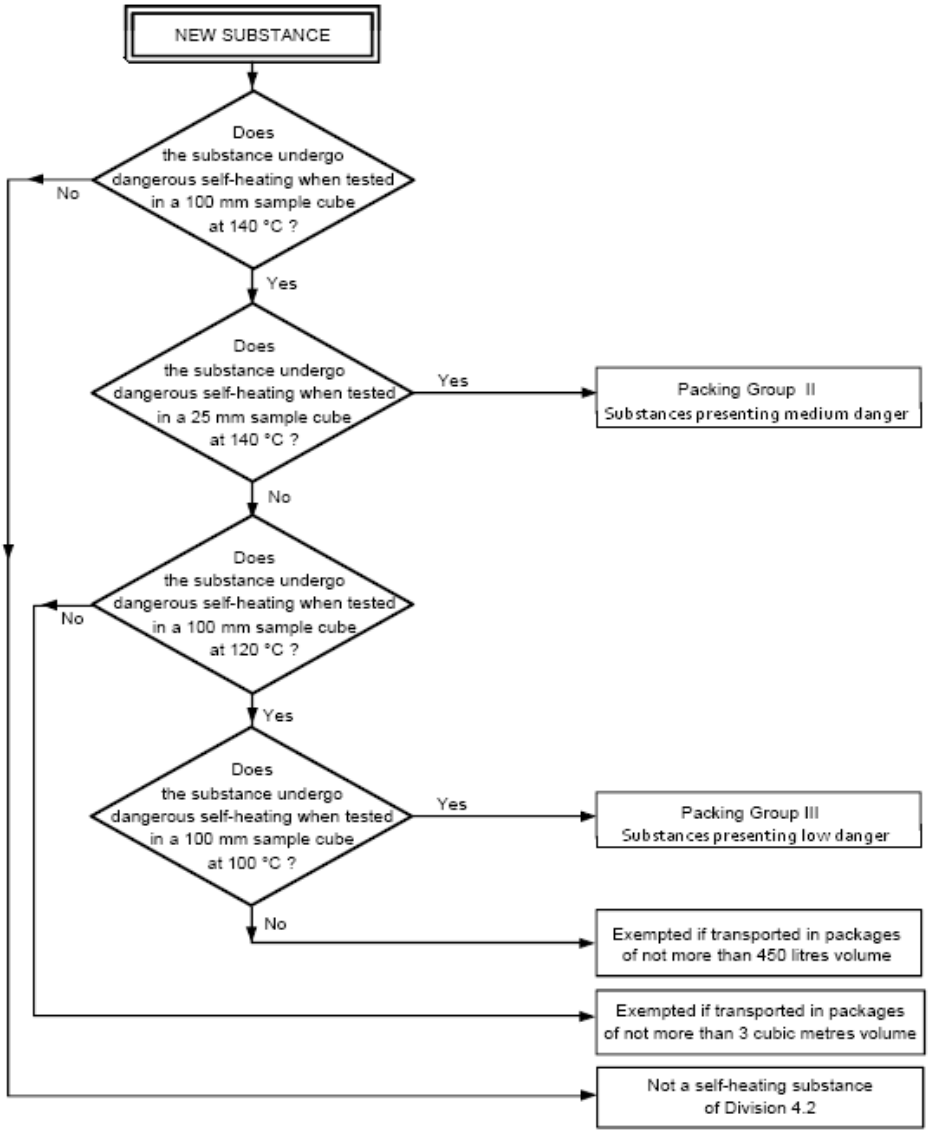

Figure 2.3: Flowsheet for the classification of self-heating substances adapted from (United Nations, 2008)

The self-heating of products such as sawdust and powdered milk has been tested using the Crossing-Point-Temperature (CPT) method (Chen, 2001). The CPT method measures the activation energy and exothermic potential of powdered materials, in an attempt to improve the basket technique employed by the U.N. Since self-heating has been shown to occur in the outer layer of samples rather than in the centre, Chen (2001) determined the crossing point temperature (T_p). The T_p is found by measuring the temperature of the sample at two points, in the

centre of the sample and a point near the centre on the same horizontal axis. The crossing-point temperature is the point at which the temperatures intersect. The T_p can then be used to obtain additional kinetic data about the material in question (Chen, 2001).

The most detailed work done on the self-heating of sulphides at low temperature was initiated in the 1980s by Rosenblum and Spira (1981) at the Noranda Technology Centre. They developed an apparatus (Figure 2.4) to measure the potential hazard of sulphide self-heating. The test samples had a mass of 1 kg with moisture content between 2-15 % mass fraction. The sample was placed in a 1 L glass vessel which was inserted inside a sealed 5 L Dewar flask and held in place by a Styrofoam block. A copper shield surrounded the Dewar which was heated to a controlled temperature of 40.0 °C ± 0.2 °C. The Dewar was maintained at standard atmospheric conditions. The rate of oxygen consumption was measured and oxygen replenished by an automatic trigger which added pure oxygen to restore standard conditions. The equilibrium temperature of an inert sample inside the Dewar is 38.5 °C. Any increase beyond this temperature indicates autogenous (i.e., self) heating. The temperature rise was measured over time to calculate a self-heating rate (°C/hr).

Some shortcomings of the system were that the sample and Dewar were heated separately and that sample size affected the self-heating rate (e.g. a 0.5 kg sample gave a 40 % higher heating rate than a 1 kg sample). It was assumed that in smaller samples almost the entire bulk contributed to heat production while in larger samples mainly the top part generated heat while the bottom part acted as a heat sink.

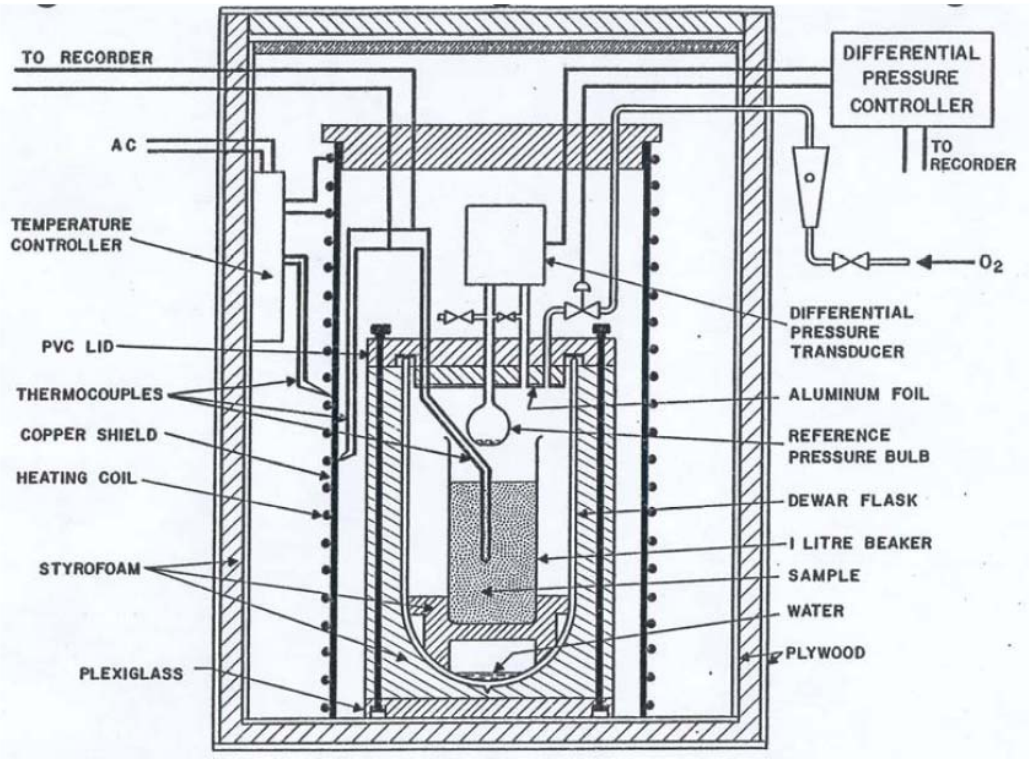

Figure 2.4: Cross-section of the temperature rise vessel (Rosenblum and Spira, 1981)

The findings led to a series of equipment and procedural improvements (Rosenblum and Spira, 1995; Rosenblum et al., 2001). The system was transferred to McGill University in 2003 when the Noranda Technology Centre was closed. It involves individual furnace units with settings and data collection by a dedicated computer. The set-up is referred to as the 'standard self-heating apparatus'. The standard test employs two stages, stage A at 70 ^{o}C, followed by stage B at 140 ^{o}C. The apparatus and test procedure is described in detail in Chapter 3.

It is understood that certain conditions, e.g. temperature and moisture level, lead to self-heating; these conditions are referred to as 'weathering'. In that sense, stage A in the standard test represents a fixed weathering condition. Recent work has been to further examine the weathering conditions that lead to self-heating (Wang, 2007; Wang et al., 2009). Weathering apparatus I (Figure 2.5) was

designed to measure sample weight gain under various controlled air conditions. Weathering apparatus II (Figure 2.6) is more sophisticated, in which air and nitrogen mixtures are used to control oxidation conditions. Temperature and relative humidity sensors are included. Weathering apparatus II has now evolved into a multi-unit set-up with full computer control. With either device, once the samples have been weathered, they are tested at the stage B (140 °C) conditions in the standard self-heating apparatus. Among the initial findings, both weathering devices I and II show that self-heating is enhanced by low oxygen levels (5 % gives higher self-heating rate than 21 %) and that the highest self-heating rates are not related to the highest rate of sample weight gain (Wang, 2007; Wang et al., 2009).

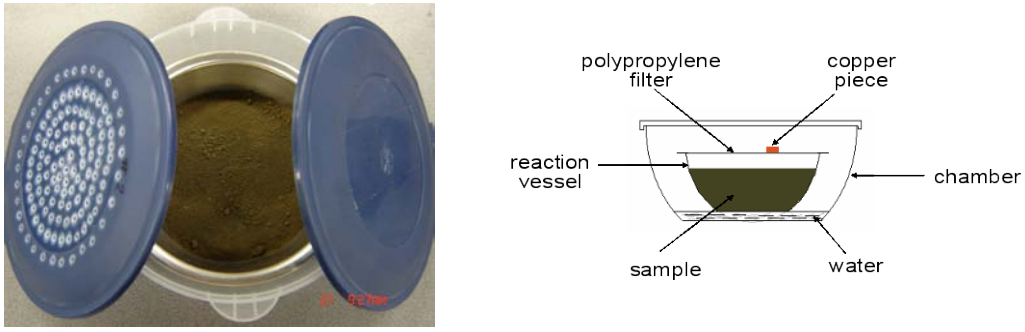

Figure 2.5: Weathering apparatus I, left image is the schematic diagram and right image is the multiple and no-hole lids (Wang et al., 2009). Reprinted with permission of the Canadian Institute of Mining, Metallurgy and Petroleum

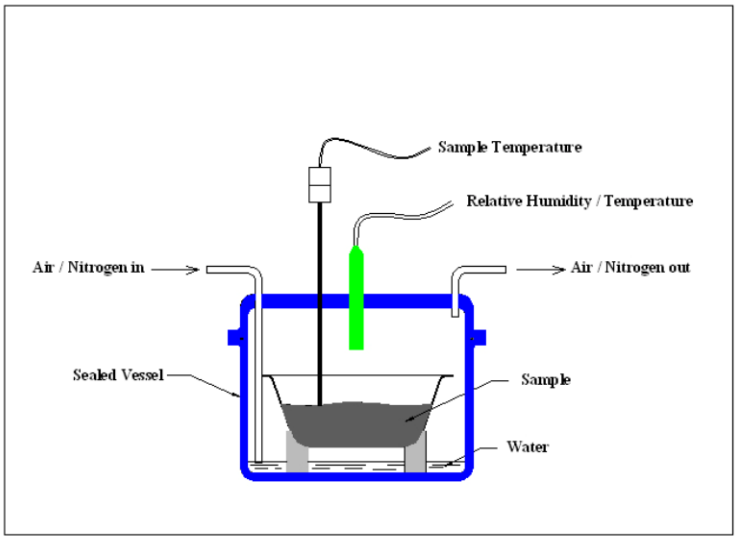

Figure 2.6: Weathering apparatus II, monitored air and sample temperature, relative humidity and control of air and nitrogen gas mixture (Wang et al., 2009). Reprinted with permission of the Canadian Institute of Mining, Metallurgy and Petroleum

2.2. Mitigation of Self-Heating

There have been several approaches to mitigation over the years. Some self-heating experiences were related to blasting of ore, which exposed surfaces to air and moisture. The problem, if caught in time, could be solved by removing the broken ore (Farnsworth, 1977; Headley et al., 1977). Underground experience also taught not to use water for dust control because it could promote self-heating and cementing of the ore (Lukaszewski, 1973; Headley et al., 1977). At Inco (now Vale), measures taken to safeguard against self-heating included improved ventilation, protocols for fire prevention and for early detection and rapid extinguishing of fires or damping of hot spots (Stachulak, 1994). Above ground, the installation of plastic covers on stockpiles proved an effective way to control self-heating by reducing access to air (Tributsch and Gerischer, 1976; Wegener and Schlieper, 1977; Rosenblum and Spira, 1995).

The use of chemicals to prevent self-heating has been considered. For example, Rosenblum and Spira (1981) added 3 lb/ton (1.34 kg/t) copper sulphate to a

sulphide sample and the self-heating rate reduced by 50 %. A suggested mechanism came later when Somot and Finch (2006, 2010) proposed that H_2S formation and subsequent oxidation was part of the chain of reactions involved in self-heating (the 'H_2S hypothesis', see section 2.4.2). By adding copper sulphate the copper reacts with H_2S to form copper sulphide (sulphidization) which effectively removes H_2S by providing a competing reaction, and suppresses the self-heating.

Another mitigation proposal is to coat sulphides using reagents to restrict access to oxygen. Two reagents were tried by Rosenblum and Spira (1995), Alconox, a laboratory detergent, and Marasperse, a commercial lignosulphonate. The self-heating rates of coated samples were significantly reduced (Figure 2.7). Polyamines have been tested as coating agents on pyrrhotite and pyrite samples (Chen et al., 2006). All samples coated with triethylenetetramine (TETA) and diethylenetriamine (DETA) showed a significant decrease in oxidation. Another approach involving chemicals was to make the moisture in sulphide samples alkaline to try to form impervious oxy-hydroxide layers to slow the reaction (Tributsch and Gerischer, 1976).

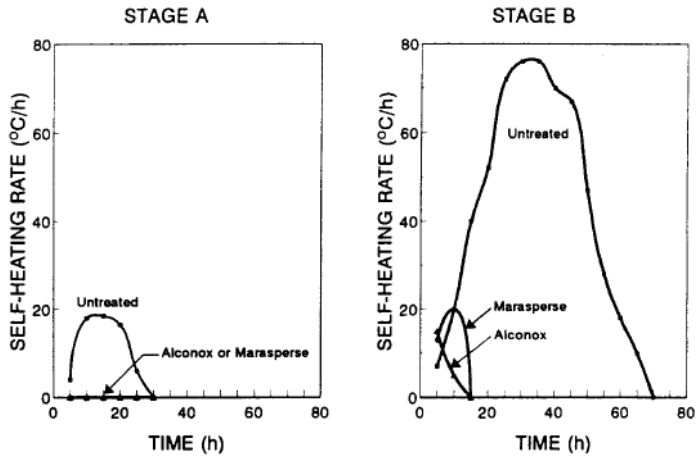

Figure 2.7: Effect of coatings on self-heating rate (Rosenblum and Spira, 1995). Reprinted with permission of the Canadian Institute of Mining, Metallurgy and Petroleum

Wu et al. (2001) tested the use of oxidation suppressants on sulphide ores (Table 2.1). The method used a 40 g sample of particle size -40 mesh (-0.45 mm). The sample was placed on a 50 mm diameter glass evaporation dish. A volume of 8 mL of suppressant was sprayed on the sample at four different aqueous concentrations (mass fractions of 0, 10, 20 and 30 %). The samples were then placed in a constant humidity chamber at a temperature of 40 °C and 90 % relative humidity. The samples were left for 4-10 days and weighed on a daily basis. The efficiency of the suppressants was assessed using Equation 2.2.

$$R_{ijt} = \left(\frac{P_{jt} - P_{ijt}}{P_{jt}} \right)(100) \qquad (2.2)$$

where R_{ijt} is the efficiency of suppressant i on ore j after time t, P_{jt} is the weight increase of ore j without adding suppressant after time t and P_{ijt} is the weight increase of sample j after adding suppressant i after time t. The results showed suppression did occur at a concentration of 10 % (and above) for suppressants A, B and C. Suppressants A and B are gels and are used commercially to prevent oxidation and extinguish fires. Suppressant action had a limited duration:

Suppressants B and C were 100 % successful for 33 days, A for 20 days and D for 11 days.

Table 2.1: List of suppressants (Wu et al., 2001)

Sample Name	Supressing Agents (mass fractions)
A	50 % $Na_2SiO_3 \cdot 9H_2O$ + 50 % $CaCl_2$
B	50 % MgO + 50 % $MgCl_2$
C	$Na_2SiO_3 \cdot 9H_2O$
D	$CaCl_2$

The suggested application of an electrochemical approach, based on its use to suppress corrosion, is to introduce electrodes in stockpiles and apply a protective electrical potential (Tributsch and Gerischer, 1976; Wegener and Schlieper, 1977).

2.3. Factors Affecting Self-Heating

2.3.1. Pyrrhotite Compared to Other Sulphides

On many occasions, pyrrhotite has been recorded as the most reactive self-heating sulphide and therefore, requires special attention (Good, 1977). It is the second most abundant sulphide mineral after pyrite (Belzile et al., 2004). Pyrrhotite is a common gangue mineral in copper and nickel deposits and a component in wastes from mining many base and precious metal ores (Cruz et al., 2005). Compared to other sulphides, pyrrhotite has a non-stoichiometric composition denoted as $Fe_{1-x}S$ where x can vary from 0 to 0.125 giving end-member molecular formulae FeS and Fe_7S_8, respectively (Thomas et al., 2001; Belzile et al., 2004; Gunsinger et al., 2006).

The symmetry of the pyrrhotite crystal lattice varies with iron content. The least iron deficient structures are associated with hexagonal or orthorhombic symmetries whereas high iron deficient structures have monoclinic symmetry. On a mole basis, the iron content for monoclinic symmetry ranges from 46.5-46.8 % Fe and for hexagonal symmetry ranges from 47.4-48.3 % Fe. The hexagonal

structure of pyrrhotite is closed packed and generally classified as NiAs type (Thomas et al., 2001; Belzile et al., 2004; Gunsinger et al., 2006). It has been documented that hexagonal pyrrhotite is more reactive then monoclinic pyrrhotite (Orlova, 1988; Belzile et al., 2004), although it is rare to find pure monoclinic or hexagonal pyrrhotite.

Pyrrhotite oxidation reaction mechanisms and kinetics are poorly understood, but it is clear that the reaction rate is greater than that of pyrite (Steger, 1982). Pyrrhotite was found to oxidise 20-100 times faster than pyrite which is attributed to its non-stoichiometric structure (Shaw, 1998). Some researchers claim that the oxidation rate of pyrrhotite increases with increasing sulphur to iron ratio (Vanyukov, 1979; Meng et al., 1993).

2.3.2. Oxygen and Moisture

Studies on sulphide oxidation at ambient temperature have all concluded that a certain level of humidity promotes reaction (Bowes, 1954; Habashi, 1966; Tributsch and Gerischer, 1976). Reimers and Hjelmstad (1987) observed that the level of oxygen did not have a strong effect on the ignition point of chalcopyrite and galena samples but that the presence of moisture did have a strong effect as measured by the weight gain of the samples. In the study by Rosenblum and Spira (1981), moisture was again found to be important. They observed maximum self-heating around 3-8 % moisture and no heating for bone-dry samples and at moisture levels above 26 % (Figure 2.8). This result led to the use of 6 % moisture in the standard self-heating test.

Test work on oxygen level is more limited. The evidence is that low levels of oxygen (5 % vs. 21 %) have a greater effect on self-heating (Wang, 2007; Wang et al., 2009).

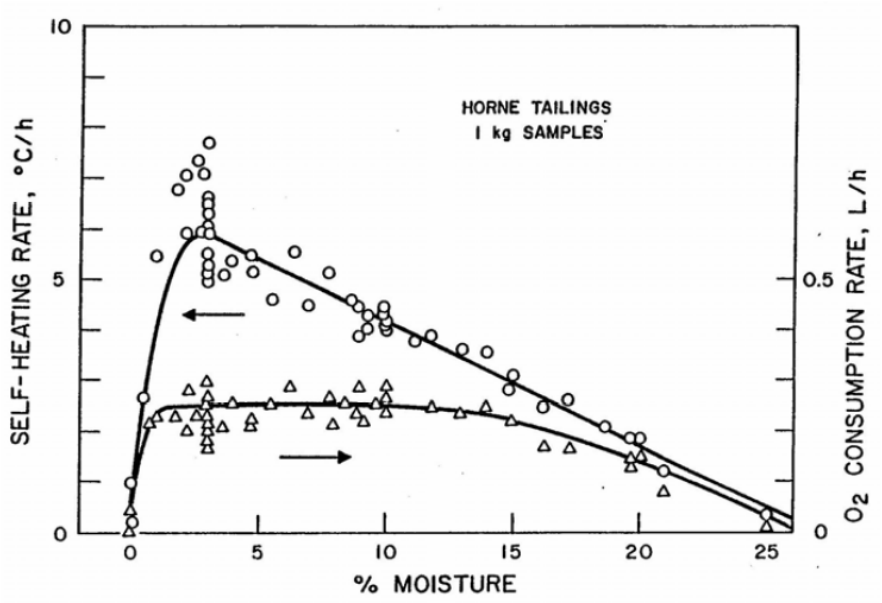

Figure 2.8: Self-heating rate and oxygen consumption against moisture content (Rosenblum and Spira, 1981)

2.3.3. Particle Size and Surface Area

It is known that the finer the iron sulphides the more problematic is self-heating (Harrington et al., 1923; Bowes, 1954). Rosenblum and Spira (1981) noted that -325 mesh (-44 μm) particles had double the heating rate of the +325 mesh size fraction. Research showed that as sulphides were ground longer (i.e., the finer they were) they could ignite or undergo weight changes at lower temperatures (Reimers and Hjelmstad, 1987). Good (1977) determined that the ignition temperature decreased with decreasing particle size. Rosenblum and Spira (1995) showed that decreasing particle size increased the self-heating rate (Figure 2.9). The observations are compatible with the fact that the finer the particle size the higher the surface area available for the oxidation reactions (Farnsworth, 1977; Ninteman, 1978; Rosenblum and Spira, 1981; Janzen et al., 2000; Kwong et al., 2003).

A study on pyrrhotite confirmed that surface area was a major factor controlling reaction kinetics (Janzen et al., 2000). Highly fractured pyrrhotite oxidises

particularly rapidly due to the increase in available surface area that may further contribute to its high reactivity compared to pyrite. It has been suggested that irregular particle shapes can also promote self-heating (Farnsworth, 1977; Janzen et al., 2000).

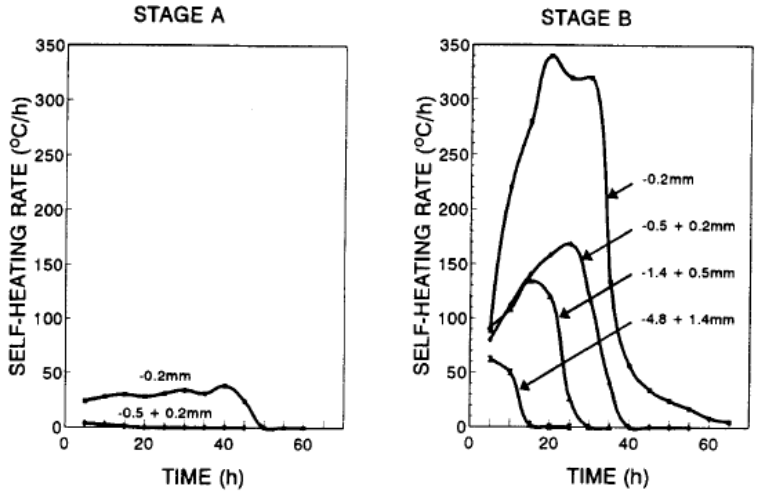

Figure 2.9: Effect of particle size on self-heating rate (Rosenblum and Spira, 1995). Reprinted with permission of the Canadian Institute of Mining, Metallurgy and Petroleum

2.3.4. Role of Iron

Iron is ubiquitous in sulphide samples and superficial oxidation always produces some iron ions in the sample moisture. Iron ions could be involved in self-heating if, as suspected (see section 2.4), electrochemical (i.e., electron transfer) reactions are at play. Ferric (Fe^{3+}) ions are electron acceptors and can be even more effective in this role than oxygen (Tributsch and Gerischer, 1976). This notion will form part of the galvanic interaction mechanism proposed in this thesis to interpret the results for sulphide mixtures.

2.3.5. Bacteria

The presence of acidophilic microorganisms such as *Thiobacillus ferrooxidans* and *Acidithiobacillus ferrooxidans* can catalyse sulphide oxidation (Gunsinger et

al., 2006). These bacteria are common in mine waste at ambient temperature and pH values below 4 (Schippers et al., 2000; Schippers et al., 2007). The bacteria oxidize ferrous iron to ferric iron as well as sulphide to sulphur (Mehta and Murr, 1983; Natarajan, 1992; Konishi et al., 1992; Das and Mishra, 1996; Nordstrom and Southam, 1997; Mielke et al., 2003; Gunsinger et al., 2006). In the presence of acidophilic bacteria, pyrite oxidation kinetics were accelerated 30-300 fold (Nordstrom and Southam, 1997).

Acidophilic bacteria were confirmed as catalysts for the oxidation of ferrous iron in tailings rich in pyrrhotite and pentlandite (Norris and Parrott, 1985; Schippers et al., 2007). Mielke et al. (2003) found that chemical oxidation of ferrous iron (i.e., with molecular oxygen) at pH levels below 4 occurred more slowly than bacterial oxidation.

Mehta and Murr (1983) showed that the presence of acidophilic bacteria enhanced galvanic interaction in two-mineral systems such as pyrite-chalcopyrite and pyrite-sphalerite. For example, they reported galvanic interaction in the presence of *Thiobaccillus ferrooxidans* increased copper dissolution by a factor of 8.

While a possible role of bacteria in self-heating is sometimes raised, to date there is no evidence that bacteria do play an active role. Mitigation tests using bactericides, for example, showed no effect on self-heating (Rosenblum, unpublished work).

2.4. Self-Heating Mechanism

The sulphide self-heating reactions are not well understood. Several studies have been conducted into the mechanisms and these are reviewed. The focus in the literature has been on mechanisms involving pyrrhotite but this is expanded to include other sulphide minerals and the possible role of electrochemical reactions.

2.4.1. Mechanisms Involving Pyrrhotite (Po)

The self-heating of sulphides has been associated with the oxidation of pyrrhotite (Kirshenbaum, 1968; Good, 1977; Ninteman, 1978; Steger and Desjardins, 1980; Meng et al., 1993; Rosenblum and Spira, 1995; Belzile et al., 2004). Among the reactions proposed the most common appear to be the following:

$$4FeS + 7O_2 \rightarrow 2Fe_2O_3 + 4SO_2 \quad (2.3)$$

$$Fe_7S_8 + O_2 \rightarrow xFeS_2O_3 + (1\text{-}x)FeSO_4 \quad (2.4)$$

$$4FeS + 3O_2 + 2H_2O \rightarrow 4FeO(OH) + 4S \quad (2.5)$$

$$FeS + 2O_2 + 7H_2O \rightarrow FeSO_4 \cdot 7H_2O \quad (2.6)$$

$$Fe_{1-x}S + (2\text{-}0.5x)O_2 + xH_2O \rightarrow (1\text{-}x)Fe^{2+} + SO_4^{2-} + 2xH^+ \quad (2.7)$$

The oxidation rate will change with temperature and relative humidity (RH). Tests conducted by Steger (1982) on pyrrhotite found that at 50 °C and 37 % RH the oxidation reaction produces sulphate (Equation 2.4). The presence of moisture (Equations 2.5, 2.6 and 2.7), allows Equations 2.3 and 2.4 to occur at temperatures close to ambient around 25 °C (Steger and Desjardins, 1978; Ninteman, 1978; Meng et al., 1993; Janzen et al., 2000; Wu and Li, 2005; Wang et al., 2009; Somot and Finch, 2010). Wu and Li (2005) noted that no SO_2 or other volatile matter is released; therefore the sample weight should increase with oxidation time.

Rosenblum and Spira (1995) noted that when self-heating occurred at low temperature (70 °C, i.e., stage A in the standard test) it continued until all moisture was exhausted. They proposed that during low temperature heating a moist sample produces elemental sulphur that fuels the self-heating when the sample is subsequently heated to 140 °C in stage B of the standard test. Self-heating in stage B is observed until the sample is exhausted of elemental sulphur. The detected oxidation products of pyrrhotite in stage A were sulphur, goethite and hematite. Contrary to Wu and Li (2005) who assumed no volatiles, the

formation of sulphur dioxide (SO_2) began around 100 °C and the self-heating rate followed the evolution of SO_2 (Rosenblum and Spira, 1995).

In natural water environments at pH > 4, oxygen is the main oxidant of sulphide minerals; however, when the pH drops below 4, sulphides also begin to be oxidised by ferric iron (Belzile et al., 2004). Pyrrhotite is known to oxidize via ferric iron in the presence of water (Good, 1977; Meng et al., 1993; Janzen et al., 2000; Gunsinger et al., 2006). While ferric iron is a more reactive oxidising agent than oxygen under acidic conditions (Moses et al., 1987) both are important oxidizing agents (i.e., electron acceptors).

$$FeS + Fe_2(SO_4)_3 \rightarrow 3FeSO_4 + S \quad (2.8)$$

$$Fe_{1-x}S + (8-2x)Fe^{3+} + 4H_2O \rightarrow (9-3x)Fe^{2+} + SO_4^{2-} + 8H^+ \quad (2.9)$$

Pyrrhotite can dissolve quickly in acidic conditions and release products such as ferrous iron and hydrogen sulphide (H_2S) (Equation 2.10) (Good, 1977; Meng et al., 1993; Belzile et al., 2004; Gunsinger et al., 2006; Somot and Finch, 2010). The oxidative dissolution mechanism of pyrrhotite in acidic media is given in Equation 2.11 (Thomas et al., 2001).

$$FeS + H_2SO_4 \rightarrow FeSO_4 + H_2S \quad (2.10)$$

$$Fe_{1-x}S \rightarrow yFe^{2+} + Fe_{1-(x-y)}S + 2ye^- \quad (2.11)$$

It is also possible that both oxygen and ferric iron partially oxidize pyrrhotite to produce elemental sulphur or an iron-deficient (polysulphide) surface-rich pyrrhotite (Steger, 1982; Janzen et al., 2000; Gunsinger et al., 2006).

$$Fe_{1-x}S + ½(1-x)O_2 + 2(1-x)H^+ \rightarrow (1-x)Fe^{2+} + S^o + (1-x)\,H_2O \quad (2.12)$$

$$Fe_{1-x}S + 2yFe^{3+} \rightarrow 3yFe^{2+} + Fe_{1-x-y}S \quad (2.13)$$

$$Fe_{1-x}S + (2-2x)Fe^{3+} \rightarrow (3-3x)Fe^{2+} + S^o \quad (2.14)$$

$$Fe_{1-x}S_{(s)} + Fe^{3+}{}_{(aq)} + ¾O_{2(aq)} + 5/2H_2O_{(l)} \rightarrow 2FeOOH_{(s)} + S^o{}_{(s)} + 3H^+{}_{(aq)} \quad (2.15)$$

From a mass balance on sulphate and iron Janzen et al., (2000) estimated that 80-86 % of the oxidised sulphide formed elemental sulphur. They also showed that ferric iron oxidation rates surpassed all other reaction rates including those involving oxygen.

As mentioned previously, the presence of iron ions is ubiquitous in moisture associated with iron sulphide systems. Both ferrous and ferric forms can react with oxygen, water and acid as in Equations 2.16-2.20 (Good, 1977; Meng et al., 1993; Janzen et al., 2000; Wu and Li, 2005).

$$2Fe^{3+} + 6H_2O \rightarrow 2Fe(OH)_{3(s)} + 6H^+ \quad (2.16)$$

$$2Fe^{3+} + 2H_2O \rightarrow 2Fe(OH)^{2+} + 2H^+ \quad (2.17)$$

$$2Fe^{2+} + ½O_2 + 2H^+ \rightarrow 2Fe^{3+} + H_2O \quad (2.18)$$

$$2FeSO_4 + (2x-1)H_2O + O_2 \rightarrow 2Fe(OH)(SO_4)\cdot xH_2O \quad (2.19)$$

$$12Fe^{2+} + 6H_2O + 3O_2 \rightarrow 4Fe(OH)_3 + 8Fe^{3+} \quad (2.20)$$

If the pH is below 3 and Equation 2.18 occurs, ferric iron will remain in solution and this could form a cycle with Equations 2.13-2.15.

Hematite (Fe_2O_3), a possible reaction product, can in turn react with acid to produce another observed reaction product, sulphate, via Equations 2.21 and 2.22 (Good, 1977):

$$Fe_2O_3 + 3H_2SO_4 \rightarrow Fe_2(SO_4)_3 + 3H_2O \quad (2.21)$$

$$Fe_2O_3 + 4H_2SO_3 \rightarrow 2FeSO_4 + S + H_2SO_4 + 3H_2O \quad (2.22)$$

Steger and Desjardins (1978) studied low temperature oxidation of pyrrhotite and found that the sulphur is oxidized to sulphate (SO_4^{2-}), thiosulphate ($S_2O_3^{2-}$), elemental sulphur (S^o) and sulphur dioxide (SO_2). The relative amount depended on the conditions, i.e., temperature and relative humidity. Elemental sulphur and

sulphur dioxide can further react as in Equations 2.23-2.25 (Good, 1977; Meng et al., 1993; Gunsinger et al., 2006).

$$S_{(s)} + 3/2O_{2(aq)} + H_2O_{(l)} \rightarrow 2H^+_{(aq)} + SO_4^{2-}{}_{(aq)} \quad (2.23)$$

$$SO_2 + H_2O \rightarrow H_2SO_3 \quad (2.24)$$

$$2SO_2 + 2H_2O + O_2 \rightarrow 2H_2SO_4 \quad (2.25)$$

2.4.2. H_2S Hypothesis

Somot and Finch (2010) tracked self-heating as a function of pyrrhotite content in mixtures with silica sand, an inert diluent. They noted that the rate of self-heating increased with pyrrhotite content but the samples visibly appeared progressively less oxidized. Given the samples were exposed to the same quantity of air (oxygen) they reasoned that a high pyrrhotite to oxygen ratio meant less oxidizing conditions. These conditions promoted the formation of hydrogen sulphide as an intermediate product and the subsequent oxidation of this gas produced the heat. Hydrogen sulphide was detected by inserting a copper piece in test samples and observing the change to a black colour identified as copper sulphide. Somot and Finch (2010) proposed the formation of H_2S occurred via Equation 2.10, generalized in Equation 2.26:

$$S^{2-} + 2H^+ \rightarrow H_2S \quad (2.26)$$

If H_2S is produced, it may entirely or partially oxidise depending on the O_2/H_2S ratio and other catalysing physical or chemical factors (e.g. temperature, water content, pressure, pH). The following reactions have been proposed (Good, 1977; Somot and Finch, 2010).

$$H_2S + ½O_2 \rightarrow S^o + H_2O \quad (2.27)$$

$$H_2S_{(g)} + O_{2(g)} \rightarrow SO_{(g)} + H_2O_{(l)} \quad (2.28)$$

$$H_2S_{(g)} + 3/2O_{2(g)} \rightarrow SO_{2(g)} + H_2O_{(aq)} \quad (2.29)$$

$$H_2S_{(g)} + 2O_{2(g)} \rightarrow 2H_2SO_{4(aq)} \quad (2.30)$$

$$2H_2S_{(g)} + SO_{2(g)} \rightarrow 3/8S_{8(s)} + 2H_2O_{(l)} \quad (2.31)$$

Note that two of the reactions (Equations 2.27 and 2.31) give elemental sulphur which serves as fuel for stage B argued by Rosenblum and Spira (2005).

2.4.3. Other Sulphide Self-Heating Mechanisms

Steger and Desjardins (1978) studied the oxidation process of several sulphides at 52 °C and 68 % RH. For pyrite, they, as well as other authors (Meng et al., 1993), proposed the following reactions

$$2FeS_2 + 3O_2 \rightarrow 2FeS_2O_3 \quad (2.32)$$

$$2FeS_2 + 4O_2 \rightarrow 2FeSO_4 + 2S^o \text{ or } 2FeS_2 + 6O_2 \rightarrow 2FeSO_4 + 2SO_{2(g)} \quad (2.33)$$

$$4FeS_2 + 11O_2 \rightarrow 2Fe_2O_3 + 8SO_2 \quad (2.34)$$

These reactions are accelerated in the presence of moisture (Ninteman, 1978; Meng et al., 1993; Wu and Li, 2005):

$$2FeS_2 + 7O_2 + 2H_2O \rightarrow 2FeSO_4 + 2H_2SO_4 \quad (2.35)$$

$$4FeS_2 + 15O_2 + 8H_2O \rightarrow 2Fe_2O_3 + 8SO_4^{2-} + 16H^+ \quad (2.36)$$

Equations 2.32-2.36 apply at ambient temperature. In oxygen-rich moisture, Equation 2.37 might occur instead of Equation 2.35. In neutral or basic conditions, Equation 2.38 is favoured:

$$4FeS_2 + 15O_2 + 2H_2O \rightarrow 2Fe_2(SO_4)_3 + 2SO_4^{2-} + 4H^+ \quad (2.37)$$

$$FeS_2 + 3H_2O \rightarrow Fe(OH)_3 + S_2 + 3H^+ + 3e^- \quad (2.38)$$

$$4FeS_2 + 15O_2 + 14H_2O \rightarrow 4Fe(OH)_3 + 8H_2SO_4 \quad (2.39)$$

For chalcopyrite, Steger and Desjardins (1978) proposed the following reactions:

$$CuFeS_2 + 2O_2 \rightarrow FeS_2O_3 + CuO \quad (2.40)$$

$$4CuFeS_2 + 7.5O_2 \rightarrow 2FeS_2O_3 + 2Cu_2S_2O_3 + Fe_2O_3 \quad (2.41)$$

$$4CuFeS_2 + 15.5O_2 \rightarrow Fe_2(SO_4)_3 + Fe_2O_3 + 4CuSO_4 + S^o \quad (2.42)$$

Steger and Desjardins (1980) also proposed oxidation reactions for galena (Equation 2.43), for sphalerite (Equation 2.44) and for iron-bearing sphalerite (Equation 2.45):

$$PbS + 2O_2 \rightarrow PbSO_4 \quad (2.43)$$

$$ZnS + 2O_2 \rightarrow ZnSO_4 \quad (2.44)$$

$$Zn(Fe)S + O_2 + H_2O \rightarrow ZnSO_4 + (Fe_2O_3 \cdot nH_2O) + S^o \text{ or } SO_2 \quad (2.45)$$

2.4.4. Electrochemical Mechanism

Habashi (1966) proposed that the mechanism of sulphide oxidation in water is electrochemical. He based this reasoning on corrosion principles, where the analogy is that imperfections in the sulphide crystal lattice would allow for anodic and cathodic sites to form. Electrons are released from the anode site (Equation 2.46 for a general metal sulphide, MeS, and Equation 2.47 for sphalerite as an example) and flow to the cathode site where oxygen is reduced (Equation 2.48):

$$MeS \rightarrow Me^{2+}_{(aq)} + S^o + 2e^- \quad (2.46)$$

$$ZnS \rightarrow Zn^{2+} + S^o + 2e^- \quad (2.47)$$

$$½O_2 + H_2O + 2e^- \rightarrow 2OH^- \quad (2.48)$$

The electrochemical behaviour of all sulphides (e.g., pyrite chalcopyrite and galena is similar). At the sulphide mineral anode site, according to Equation 2.46, elemental sulphur is formed and metal ions are released into the electrolytic solution (i.e., the sample moisture in the present situation).

The cathodic reaction in Equation 2.48 specifies oxygen but other electron acceptors, such as ferric iron (Fe^{3+}) as seen in Equation 2.49 can be substituted (Tributsch and Gerischer, 1976). The principal electron acceptor is ferric iron:

$$Fe^{3+} + e^{-} \rightarrow Fe^{2+} \quad (2.49)$$

Harmer et al. (2006) examined the evolution of surface layers during chalcopyrite leaching and proposed that reaction was via surface polysulphides, S_n^{2-}, Equation 2.50 and/or 2.51 (with S_2^{2-} i.e., n = 2, representing the polysulphides). Ferric iron was considered reduced to ferrous iron via Equation 2.49 and then reacted as in Equation 2.52 to regenerate ferrous and form a cycle promoting chalcopyrite dissolution (Harmer et al., 2006).

$$S_2^{2-} + 2Fe^{2+} + 2H^{+} \rightarrow H_2S + 2Fe^{3+} + S^{2-} \quad (2.50)$$

and/or

$$S_2^{2-} + 2Fe^{2+} \rightarrow 2S^{2-} + 2Fe^{3+} \quad (2.51)$$

$$S^{2-} + 2Fe^{3+} \rightarrow S^{o} + 2Fe^{2+} \quad (2.52)$$

Thomas et al. (2001) and Harmer et al. (2006) proposed a similar mechanism, both suggesting the reduction of polysulphide (S_n^{2-}) to sulphide (S^{2-}) as ferrous iron is oxidized to ferric iron. Harmer et al. (2006) proposed that Equation 2.50 is driven by the oxidation of ferrous iron to ferric iron, while H^{+} is adsorbed and Thomas et al. (2001) attributed Equation 2.50 to an electron accumulation. The two products (Equations 2.50 and 2.51) indicate the possibility of both S^{2-} and H_2S forming.

While both Thomas et al. (2001) and Harmer et al. (2006) suggest the formation of H_2S, Harmer et al. (2006) went further to propose that ferric iron formed by the reduction of polysulphide by ferrous iron (Equation 2.50) is re-generated as ferrous by Equation 2.49, forming an oxidative-reductive cycle favouring the formation of H_2S. Harmer et al. (2006) did detect H_2S in their experiments.

Tributsch and Gerischer (1976) suggested that the oxidation of sulphides in contact with moisture and oxygen follows a mixed mechanism, where the initial steps are electrochemical (e.g. reduction of O_2 and Fe^{3+} as in Equations 2.48 and 2.49, respectively) and the subsequent steps are chemical (e.g. sulphate formation). They reasoned that at ambient temperatures, direct chemical attack by oxygen (O_2) is unlikely due to the high dissociation energy required to break the O_2 molecule. They proposed that since the sulphides are semiconductors, an electron is transferred from the solid to the oxygen (O_2) as the cathodic reaction in the sequence and produces hydrogen peroxide (H_2O_2) as an intermediate. The formation of sulphate is the final stage of oxidation. Their Equations 2.53 and 2.54 suggest that sulphate formation is due to the H_2O_2 intermediate:

$$S + O_2 \rightarrow SO_2 + H_2O \rightarrow H_2SO_3 \quad (2.53)$$

$$H_2SO_3 + H_2O_2 \rightarrow H_2SO_4 + H_2O \quad (2.54)$$

2.5. Electrochemical Processes Involving Sulphide Minerals

Most sulphide minerals are electrically conducting. Consequently, when a sulphide mineral is placed in an aqueous electrolyte (the situation with all process waters) it becomes an electrode. This can be demonstrated when a mineral is connected with a reference electrode and a potential is recorded. This potential is called the open circuit or rest-potential, measured once the sulphide is at equilibrium with its surroundings (Rao and Leja, 2004). The electrochemical behaviour of sulphide minerals is characterised by their rest-potential (Kwong et al., 2003). A list of rest-potentials is found in Table 2.2. The values vary depending on the origin of the mineral but the order generally remains consistent:

Pyrite > Chalcopyrite > Sphalerite > Pentlandite > Pyrrhotite > Galena

To illustrate the importance of the order, consider two sulphides in contact in the presence of electrolyte. The sulphide with the lower rest-potential acts as the anode and undergoes oxidation by giving up electrons to the sulphide with the higher rest-potential acting as the cathode. The final electron acceptor is commonly oxygen, which is reduced to hydroxide (OH^-) in Equation 2.48, or, as noted, sometimes Fe^{3+}, which is reduced to Fe^{2+} (Equation 2.49) (Rao and Finch, 1988; Leja and Rao, 2004). This electrochemical process is known as galvanic interaction.

Table 2.2: Rest Potential Values (Kocabag, 1985)

Mineral	Formula[1]	Rest Potential vs. S.H.E. (Volts)
Pyrite	FeS_2	0.66
Chalcopyrite	$CuFeS_2$	0.56
Sphalerite	ZnS	0.46
Pentlandite	NiFeS	0.35
Pyrrhotite	FeS	0.31
Galena	PbS	0.28

[1]Nominal formula, natural samples can vary.

A specific example of galvanic interaction is illustrated in Figure 2.10 for pyrite and sphalerite. From Table 2.2 the rest-potential of pyrite (0.66 V) is higher than that of sphalerite (0.46 V). Therefore, galvanic interaction occurs where electrons flow from sphalerite, the anodic mineral, to pyrite, the cathodic mineral. As the anode, sphalerite is oxidized according to Equation 2.47. The cathodic reaction is either the reduction of oxygen on the surface of pyrite as in Equation 2.48 or the reduction of ferric iron (Equation 2.49).

It is the difference in rest-potential that is the driving force for galvanic interaction. The larger the rest-potential difference the greater the probability of galvanic interaction (Rao and Finch, 1988).

In the example, the cathodic mineral is pyrite because it has the higher rest-potential of the pair of sulphides. Pyrite has the highest rest-potential of the common sulphides and, therefore, is cathodic to most other sulphide minerals. In turn, it is the least likely to oxidize (act as anode) leading to the alternative description that pyrite is the noblest sulphide (Leja and Rao, 2004).

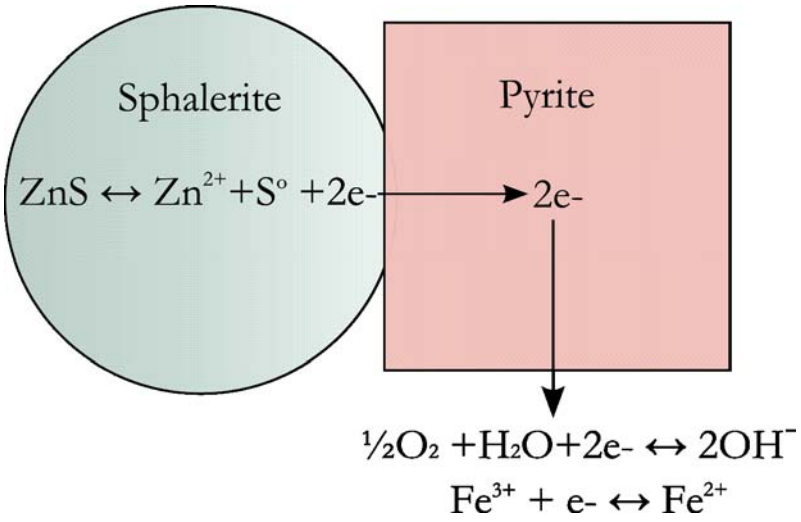

Figure 2.10: Schematic of the galvanic interaction mechanism of pyrite and sphalerite

In multi-sulphide systems, the potential measured is the overall potential which is the combination of all the electron transfer reactions occurring simultaneously in the system. This overall potential is known as the mixed potential. Minerals with rest-potential below the mixed potential will act as anodic minerals; those with rest-potential above the mixed potential will act as cathodic minerals.

Apart from the difference in rest-potential the relative surface area in contact between the sulphide particles also influences galvanic interaction. Yelloji Rao and Natarajan (1989) showed that the surface area between anode and cathode influenced the rate of reaction in a galvanic cell and identified that a large specific surface area of the cathodic mineral was the main driver. Kwong et al. (2003) came to a similar conclusion. Therefore, the larger the cathode to anode surface area ratio, the greater the galvanic interaction (i.e., higher the current density).

2.5.1. Examples of galvanic effects in sulphide systems

2.5.1.1.Mineral processing

The two main steps in mineral processing are liberation and separation. Mineral liberation is by size reduction in which ore is ground using a variety of methods. Flotation is a physico-chemical technique that employs bubbles for the separation of minerals suspended in water.

Size reduction includes grinding in tumbling mills usually under wet conditions (i.e., particles are present in a slurry) using steel balls as grinding media. In the case of sulphide minerals contact with steel grinding media can cause galvanic effects (Adam et al., 1984). When mild steel is used it is typically the material with the lowest rest-potential in the system, therefore, it forms the anode (Rao et al., 1992). As a consequence the grinding media oxidizes (i.e., corrodes) at an accelerated rate in the presence of sulphides with oxygen and ferric ions acting as the final electron acceptors (Rao et al., 1992; Leja and Rao, 2004). The release of iron ions (the oxidation products) into the aqueous environment can lead to the deposition of iron oxy-hydroxide precipitates on the mineral particles that reduces selectivity (Finch et al., 2006)

2.5.1.2.Leaching

The leaching dissolution of sulphide mixtures can be predicted from rest-potential measurements (Mehta and Murr, 1983; Natarajan, 1992). Work has shown that dissolution rates for sphalerite, chalcopyrite and galena are much faster in the presence of pyrite than when alone (Gottschalk, 1912; Abriatis et al., 2004). This phenomenon is exploited in the Galvanox^{TM} process used to enhance leaching of chalcopyrite through galvanic interactions by addition of pyrite (Dixon et al., 2007).

The electrochemically active nature of sulphides has led researchers to suspect that galvanic effects may influence sulphide self-heating (Kirshenbaum, 1968; Ninteman, 1978; Rosenblum and Spira, 1995; Wang, 2007). This forms the hypothesis tested in this thesis.

Chapter 3 Experimental Procedure

3.1. Materials and Sample Preparation

3.1.1. Pyrrhotite Containing Systems

Samples of pyrite concentrate from Xstrata Zinc's Brunswick Mine (New Brunswick), pentlandite concentrate from Vale's Clarabelle Mill and tailings high in pyrrhotite from Xstrata Nickel's Strathcona Mill (the latter two both in the Sudbury area, Ontario) were shipped wet to McGill in sealed plastic bags. The pyrrhotite samples were split and pressure filtered into cake. The cakes were freeze dried at -40 °C (courtesy of McGill Chemical Engineering Department), sealed in plastic bags and stored in a freezer. The pyrite and pentlandite samples were oven dried at 40 °C, placed in sealed bags and stored in the freezer.

3.1.2. Non-pyrrhotite Systems

Samples of chalcopyrite, sphalerite and galena as their respective Cu, Zn and Pb concentrates were obtained from Xstrata Zinc's Brunswick Mine and a sample of pyrite from Zacatecas, Mexico was purchased from Ward's Scientific. The pyrite was received as ~2-3 cm^3 chunks which were passed through a Marcy jaw crusher (10.16 cm by 5.24 cm) and reduced to -850 μm. The samples were stored in sealed plastic bags and kept in closed containers at room temperature.

The samples were passed through a 850 μm Sweco screen. Oversize (+850 μm) material was pulverized using a Siebtechnik pulverizer type T100 to pass the screen. The resulting ca. 4 kg samples were split into 10 sub-samples using a Dickie and Stockler Rotary Sample Divider.

3.1.3. 'Purer' Sulphides

Approximately 4 kg samples of pyrite (Zacatecas, Mexico), sphalerite (Balmat, U.S.A.) and galena (Morocco) were obtained from Wards Scientific, along with

high-grade chalcopyrite from Xstrata Nickel's Strathcona Mine. The materials were prepared as per the pyrite sample in section 3.1.2.

3.1.4. Controlled Particle Size Systems

Pyrite (Huanzala, Peru) and sphalerite (Balmat, U.S.A.) (ca. 6 kg of each) from Ward's Scientific were used in this work. A combination of jaw crusher and Siebtechnik pulverizer was used to reduce the as-received samples to 100 % passing 3.35 mm (Sweco screen). The resulting material was split on a Jones Riffler. Each portion of approximately 500 g was ground in a tumbling mill with (electrochemically inert) ceramic (zirconia) balls. The ball charge was 2 kg 10 mm balls, 1 kg 20 mm balls and 2 kg 30 mm balls. The grinding time was adjusted to obtain four size classes, about 80 % passing 850 μm, 300 μm, 75 μm and 38 μm. Following production of each batch, a small portion was screened to verify the target size. Dry screening was done for sizes above 75 μm and wet for sizes below 75 μm. The particle size distribution was determined using a laser particle size analyzer (HORIBA, Laser scattering particle size analyzer LA-920). The samples were stored in sealed plastic bags at room temperature.

3.2. Sample Characterization

3.2.1. X-Ray Diffraction

The composition of the powder samples was established using x-ray diffraction (Philips P1710 with rotating Cu anode set at 40 kV and 20 mA). The software for data acquisition was Expert Quantify and for phase analysis was X'Pert High Score.

3.2.2. Particle Size

Samples with particles smaller than 200 μm were measured using the HORIBA. The detection limit quoted by the manufacturer is 0.020 μm.

3.2.3. Surface Area

The surface area of the samples was measured using a BET Micromeritics TriStar 3000 Surface Area and Porosity Analyzer. The samples were degassed for 2 hours at 50 °C using a Degasser Micromeritics FlowPrep 060 Sample Degas System.

3.2.4. Atomic Absorption Spectrometry

The metal content was measured following acid digestion using a Fast Sequential Atomic Absorption Spectrometer AA240FS (Varian). The detection limit for this instrument was 0.003 mg/kg for iron, 0.002 mg/kg for copper, 0.002 mg/kg for zinc and 0.01 mg/kg for lead.

3.2.5. Induced Coupled Plasma-Optical Emission Spectrometry

An inductively coupled plasma-optical emission spectrometer (ICP-OES) was also used to assay each sample and to check the atomic absorption results. The instrument was a Trace Scan ICP-OES from Thermo Scientific set at a pump flow of 1.5 mL/min. Accessories included: a mini-cross flow nebulizer (pressure 30 psig), a mini-cyclonic spray chamber, and a hi-flow torch (1000 Watts) from SCP Science. Trace scan software was used to process data for four elements: iron, copper, zinc and lead at wavelengths 259.9 nm, 324.7 nm, 206.2 nm and 220.3 nm, respectively.

3.3. Standard Self-Heating Test

The tests were performed using the self-heating apparatus and procedure developed by Rosenblum and coworkers (Rosenblum and Spira, 1995; Rosenblum et al., 2001). A self-heating cell containing a test sample is shown in Figure 3.1. A standard self-heating test has a 530 g sample with a mass fraction of 6 % humidity (i.e. 500 g dry sample and 30 g water). The test involves two stages,

A followed by B. Stage A is held at 70 °C and stage B is held at 140 °C (i.e., below and above the boiling point of water, respectively). Both stages last 50 hours consisting of ten 5-hour cycles, each beginning with 15 minutes of air injection the air rates for stage A and B are 100 mL/min and 250 mL/min, respectively. Immediately following stage A, any condensates found in the reservoir at the bottom of the self-heating cell (Figure 3.1) are removed by a vacuum that runs for 30 seconds collecting all liquids. Nitrogen is injected into the sample at a rate of 260 mL/min during this period which allows the sample to dry for 9.5 hours and the temperature to reach 140 °C for stage B.

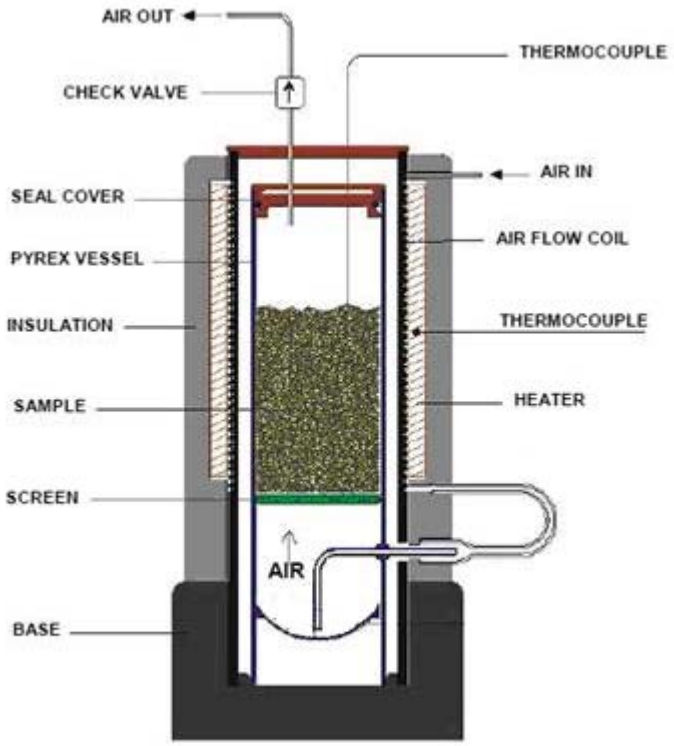

Figure 3.1: Self-heating cell for stage A and B adapted from (Rosenblum et al., 2001)

The automated program records the temperature at the centre of the sample as a function of time. Once the test is finished the recorded data are imported into the SELFHEAT software developed by Rosenblum. Figure 3.2 is a thermograph illustrating no-self-heating events and Figure 3.3 is a thermograph in which self-

heating is observed. The vertical bars in both figures represent the air-flow frequency and rate entering the self-heating cell.

Above each of the air injection points (the first 15 minutes of every 5-hour cycle) the self-heating rate (SHR) is given calculated by the SELFHEAT software. The SHR is the slope of the temperature curve at each air injection point and it is measured in units of degrees Celsius per hour (°C/hr). The sum of all the SHRs in stage A and in stage B yields the total SHR for stage A and B. The total SHR is used to calculate the self-heating capacity (SHC) according to Equation 3.1:

$$SHC = \left(\sum SHR(\frac{^\circ C}{hr}) \right) \left(SpecificHeat(\frac{J}{g^\circ C} \right) \left(InjectionTime(hr) \right) \qquad (3.1)$$

The specific heat for sulphides ranges between 0.5-0.7 J/g°C (Pankratz, 1984), and the single value chosen for these experiments was the middle of the range, 0.6 J/g°C. The air injection time is 15 minutes or 25 % of an hour. Therefore, Equation 3.1 becomes:

$$SHC = \left(\sum SHR(\frac{^\circ C}{hr}) \right) \left(0.6(\frac{J}{g^\circ C} \right) \left(0.25(hr) \right) \qquad (3.2)$$

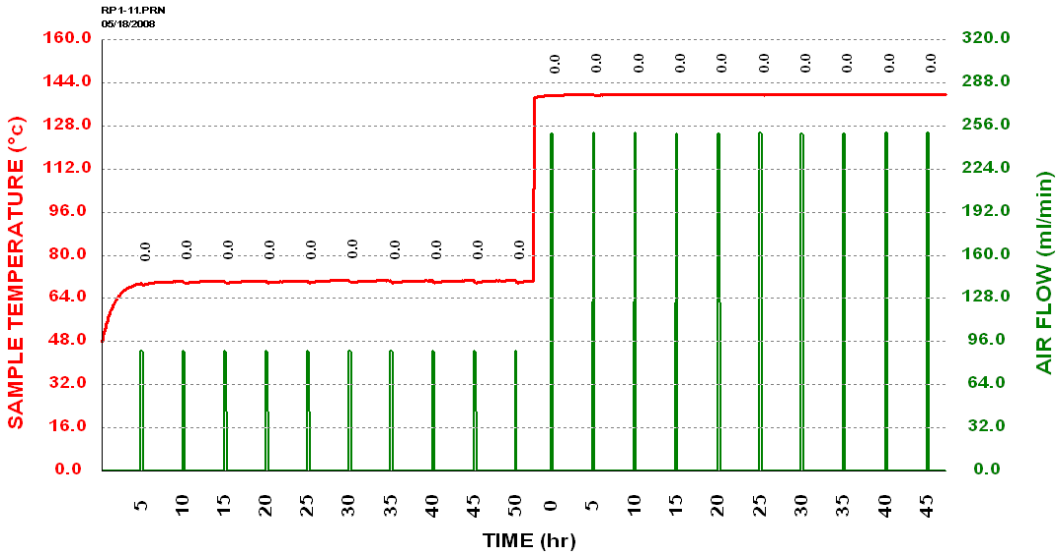

Figure 3.2: Thermograph for a non-self-heating sulphide sample

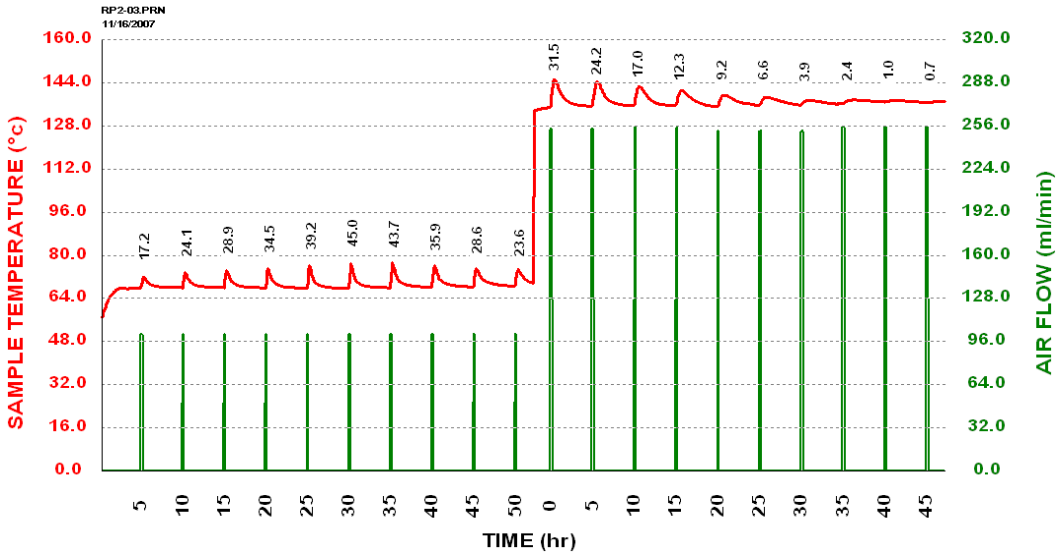

Figure 3.3: Thermograph for a self-heating sulphide sample

The results are plotted on the 'risk assessment chart' illustrated in Figure 3.4, with the SHC for stage B on the y-axis and SHC for stage A on the x-axis. From the extensive experience using the standard self-heating test, based on a sample's position on the chart, the self-heating hazard can be estimated along with the recommended action.

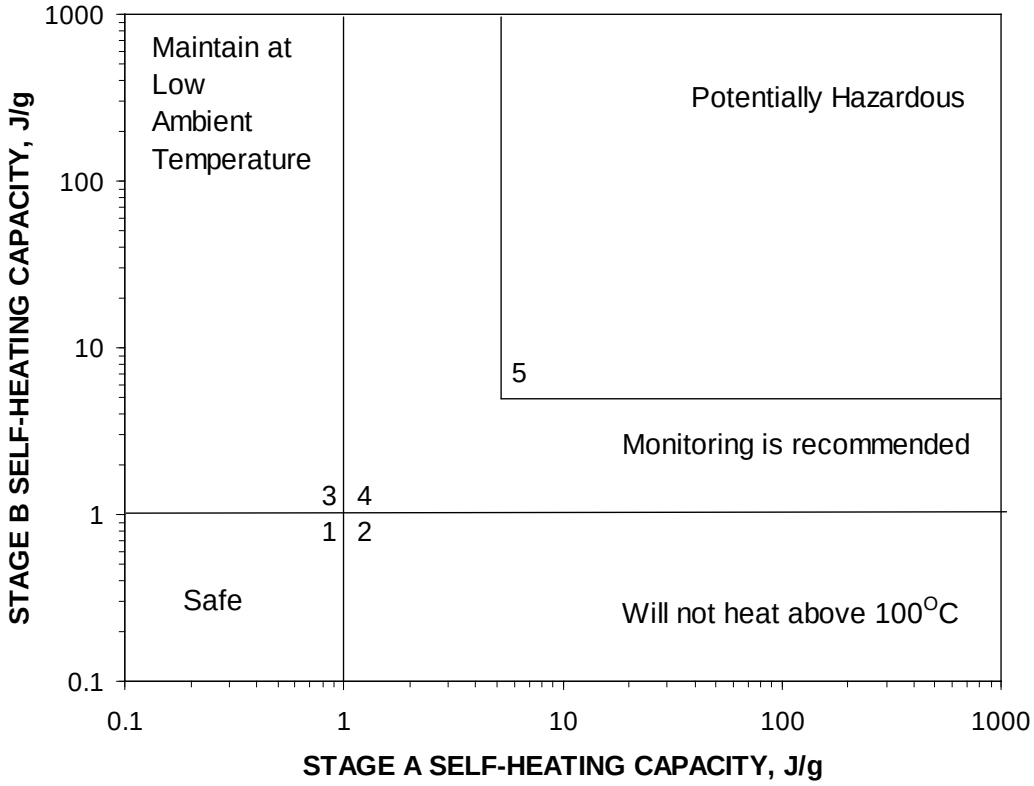

Figure 3.4: Risk assessment chart for the self-heating of sulphides

Chapter 4 Results

4.1. Sample Characterization

4.1.1. Pyrrhotite Containing Systems

The x-ray diffraction patterns for pyrite, pentlandite and pyrrhotite are given in Figure 4.1 (a), (b) and (c), respectively. The actual patterns (gray) are matched with reference patterns (black). All three patterns have unidentified peaks; keeping in mind that these samples are concentrates; they will contain other minerals besides the main sulphide. The pyrite sample contains galena as a major impurity as well as chalcopyrite and suspected willemseite (nickel magnesium silicate) as minor impurities. The pentlandite sample contains pyrite, pyrrhotite, chalcopyrite, and willemseite impurities; and the pyrhrotite sample contains serpentine, pyrite and albite (clay).

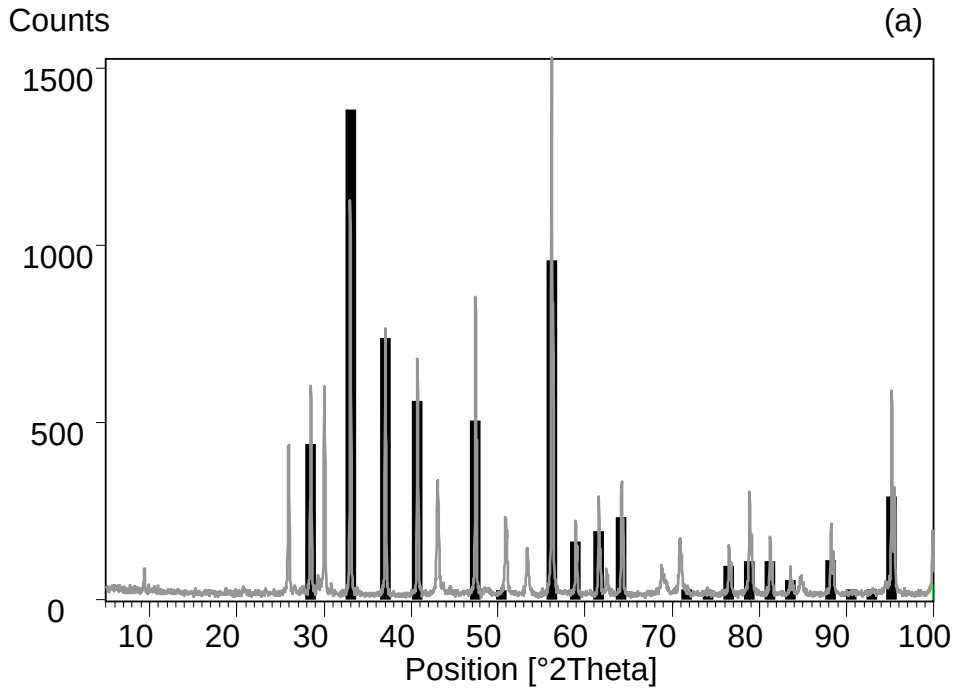

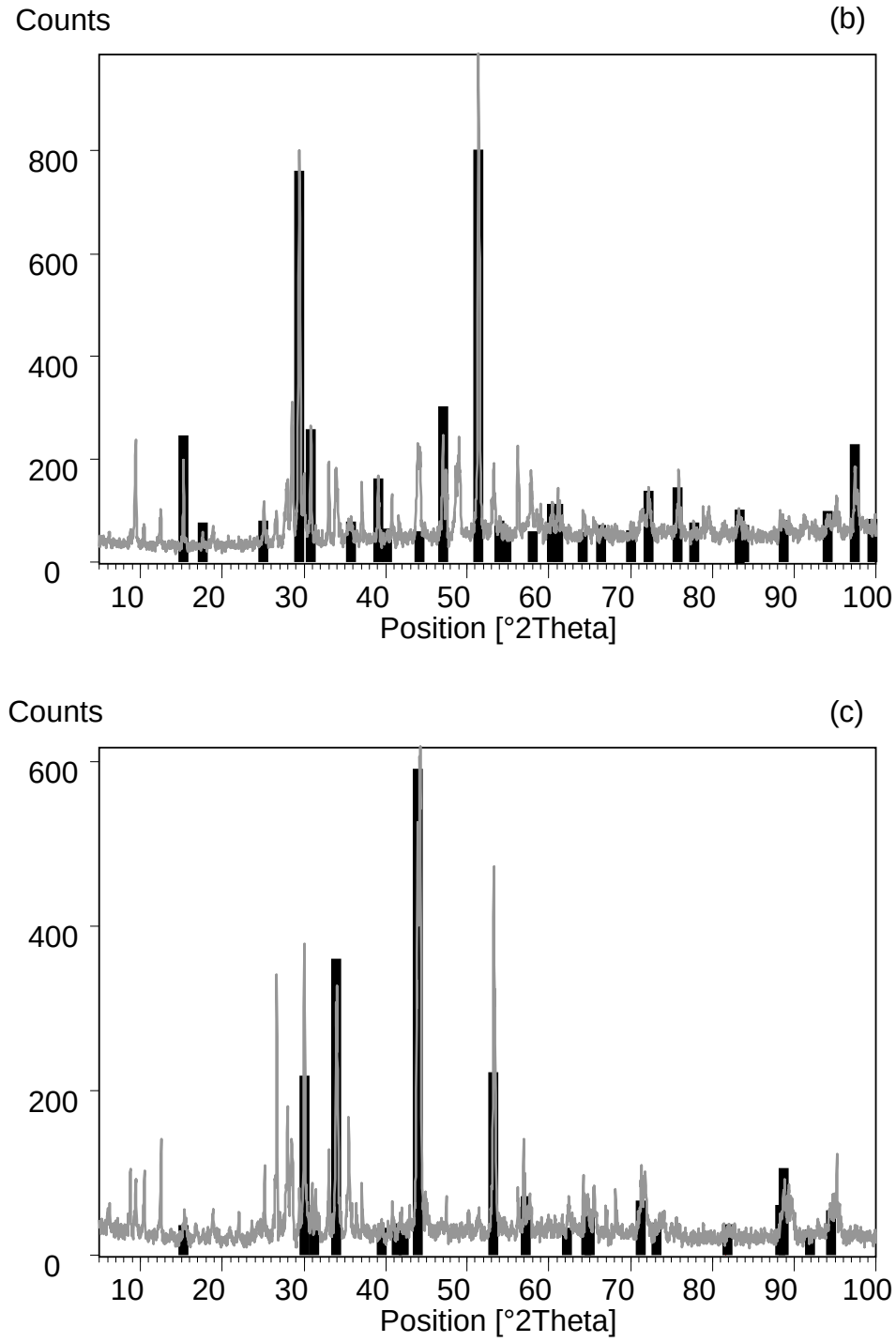

Figure 4.1: X-ray diffraction patterns for (a) pyrite, (b) pentlandite and (c) pyrrhotite

The sample particle size, given as the 80 % passing size (X_{80}), is presented in Table 4.1. The X_{80} is the mean of three repeats with the standard error of the mean (SE) indicated.

Table 4.1: Particle sizes for pyrrhotite containing systems

Sample	X_{80} (μm)	SE (μm)
Pyrite (Py)	19.9	0.6
Pentlantdite (Pn)	22	1
Pyrrhotite (Po)	24.2	0.4

4.1.2. Non-pyrrhotite Systems

The x-ray diffraction patterns for pyrite, chalcopyrite, sphalerite and galena (Appendix Figure A 1) were used to determine the main mineral impurities in each sample. Atomic absorption and induced coupled plasma-optical emission spectrometry were used to determine the assay of the main elemental constituents. These results are presented in Table 4.2.

Table 4.2: Sample purity for non-pyrrhotite systems

Sample	Main Constituent	Impurities
Pyrite	> 95 % pyrite	-
Chalcopyrite	~ 75 % chalcopyrite	galena
Sphalerite	~ 90 % sphalerite	pyrite, galena
Galena	~ 60 % galena	pyrite

The particle size data (average from 5 repeats) are found in Table 4.3.

Table 4.3: Particle size for non-pyrrhotite containing systems

Sample	X_{80} (μm)	SE (μm)
Pyrite	121	4
Chalcopyrite	51	1
Sphalerite	60	2
Galena	68	1

4.1.3. 'Purer' Sulphides

The x-ray diffraction patterns for the 'purer' sulphide samples are given in Appendix Figure A 2. The results are summarized in Table 4.4. The diopside identified in the sphalerite sample is a calcium-magnesium silicate. Atomic absorption and induced coupled plasma-optical emission spectrometry were used to determine the assay of the main constituents in each sample.

Table 4.4: Composition for samples of 'purer' sulphides

Sample	Main Constituent	Impurities
Pyrite	> 95 % pyrite	-
Chalcopyrite	~ 65 % chalcopyrite	-
Sphalerite	~ 55 % sphalerite	quartz, diopside
Galena	~ 95 % galena	-

The particle size data (average of five repeats) are recorded in Table 4.5.

Table 4.5: Particle size for 'purer' sulphide systems

Sample	X_{80} (μm)	SE (μm)
Pyrite	121	4
Chalcopyrite	89	2
Sphalerite	134	4
Galena	39	3

4.1.4. Controlled Particle Size Systems

The pyrite and sphalerite samples are those identified in Table 4.4. The particle size and the surface area (SA) for the four grind sizes are indicated in Table 4.6.

Table 4.6: Particle size for controlled particle size systems

	Pyrite			Sphalerite		
Grind Size	X_{80} (μm)	SE (μm)	SA (m^2/g)	X_{80} (μm)	SE (μm)	SA (m^2/g)
1	888	5	0.020	777	4	0.621
2	348	4	0.106	332	4	0.716
3	72	1	0.224	67	2	0.911
4	27	2	0.465	21	1	1.450

4.2. Standard Self-Heating Tests

4.2.1. Pyrrhotite Containing Systems

Binary sulphide mixtures composed of pyrite-pyrrhotite (Py-Po) and pyrite-pentlandite (Py-Pn) were tested in the standard self-heating apparatus with results compared to the sulphides tested alone. The standard sample is 500 g solid (plus a mass fraction of 6 % water, i.e., 30 g water) made up by adding silica sand (80 % -250 μm). The sample is designated by the content of sulphide: for example, in the single mineral tests 25 % Py means 25 % of the 500 g by weight (i.e., 125 g) is Py and the rest (375 g) is sand; as an example of a mixed sample, 25 % Py + 25 % Po means 125 g of both Py and Po by weight with the rest sand. The sand does not self-heat and is used as an inert diluent to extend the sample and thus the number of tests. The procedure has been used before (Somot and Finch, 2006).

The results for Py-Po in stages A and B are presented in Figure 4.2 and Figure 4.3. Each test was performed once and the error bar indicated is the standard deviation for the instrument determined in previous work (Wong, 2005).

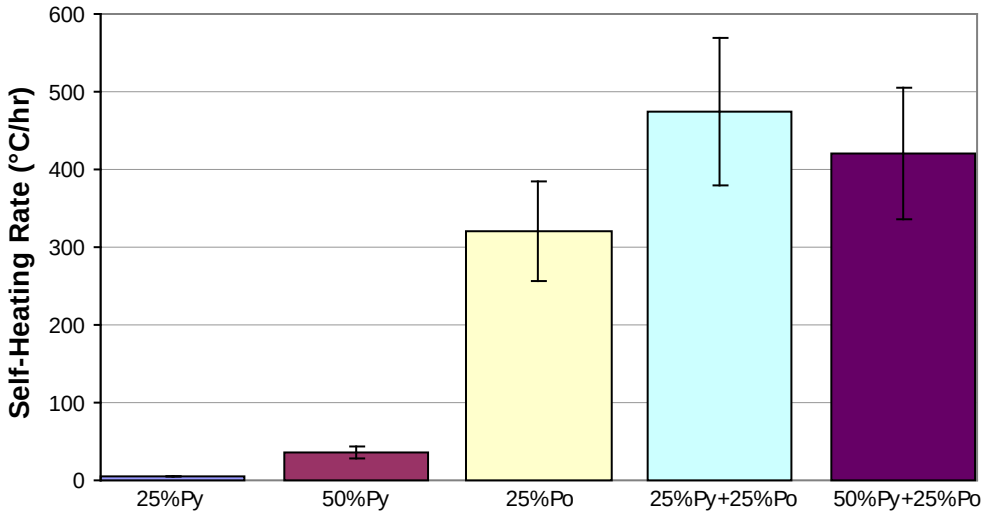

Figure 4.2: Stage A self-heating rate for pyrite and pyrrhotite alone and mixed

In stage A (Figure 4.2), pyrite alone (both 25 % Py and 50 % Py tests) self-heats only slightly, much less than pyrrhotite alone (< 50 °C/hr compared to ca. 300 °C/hr). When pyrite and pyrrhotite are combined the self-heating rate for stage A rises above 400 °C/hr. In stage B (Figure 4.3), the same trend is observed.

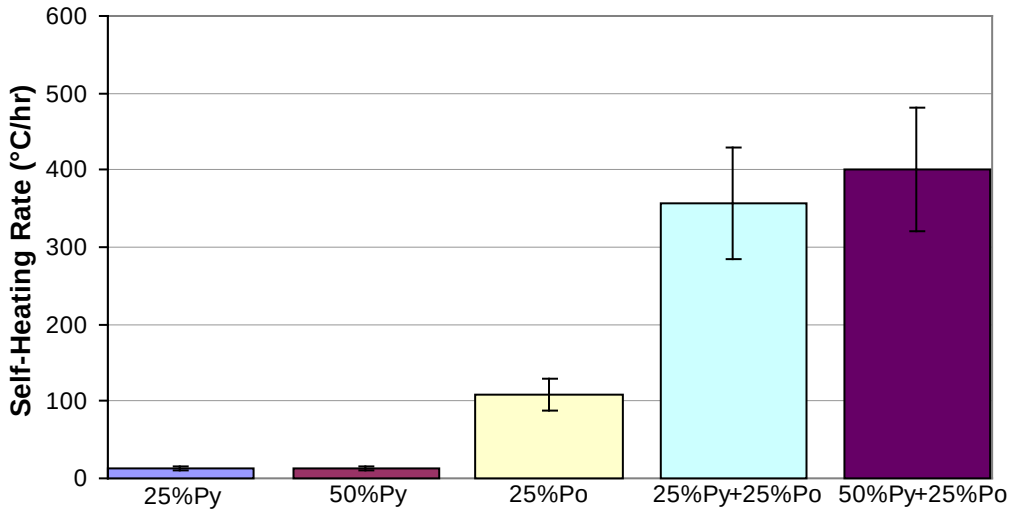

Figure 4.3: Stage B self-heating rate for pyrite and pyrrhotite alone and mixed

The same type of test was performed on the Py-Pn system. The results for stages A and B are seen in Figure 4.4 and Figure 4.5, respectively. In stage A, the self-heating rates for pyrite and pentlandite alone are below 50 °C/hr. When combined in equal proportions, the self-heating rate rises to about 250 °C/hr and further increases when the content of pyrite is doubled (to 400 °C/hr). In stage B, the same trend is observed although heating rates are lower than in stage A.

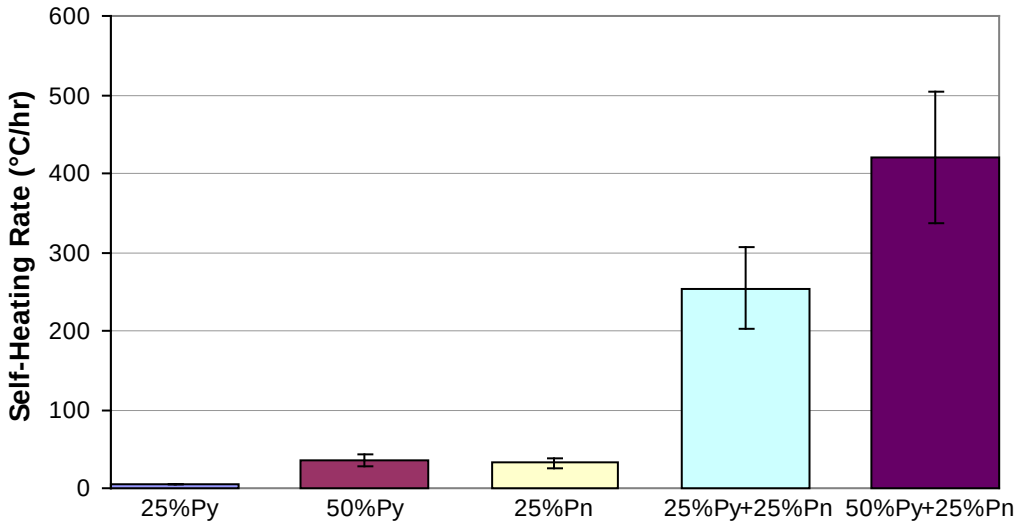

Figure 4.4: Stage A self-heating rate for pyrite and pentlandite alone and mixed

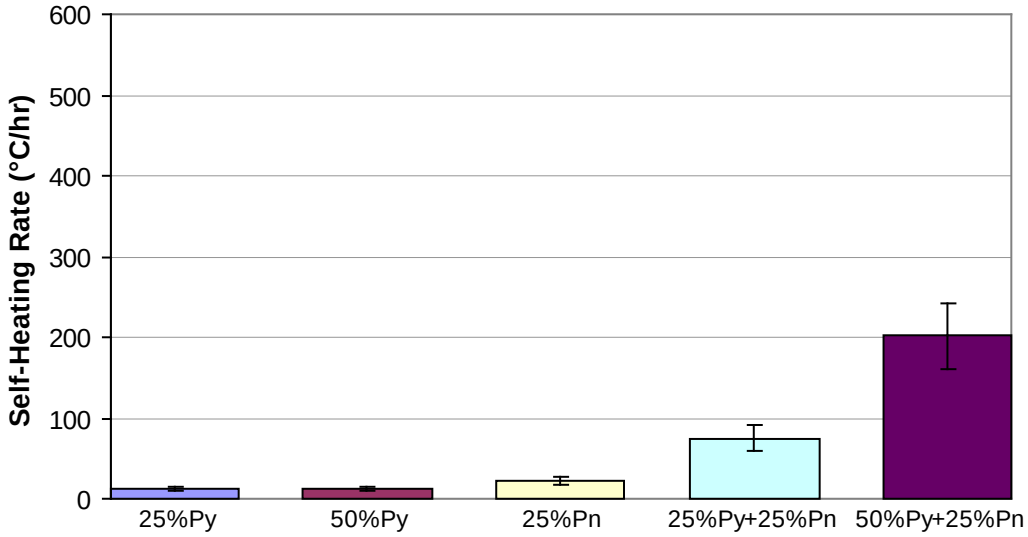

Figure 4.5: Stage B self-heating rate for pyrite and pentlandite alone and mixed

With both examples (Py-Po and Py-Pn), the self-heating of the sulphides when combined is significantly greater than when alone. This indicates galvanic

interaction. Given the known reactivity of pyrrhotite, however, tests were required to identify the galvanic effect free of this consideration.

4.2.2. Non-Pyrrhotite Systems

Four common sulphides, pyrite, chalcopyrite, sphalerite and galena, were chosen because they do not typically self-heat, which proved the case here (Appendix, Table A 2). Binary mixtures were formed according to the rest-potential differences (ΔE) using values reported in literature (Table 2.2). All mixtures contained a mass fraction of 50 % of each sulphide (i.e., 250 g each, with no sand). Two mixtures were created with high rest-potential difference, pyrite-galena (0.45 V) and chalcopyrite-galena (0.35 V), and two mixtures with low rest-potential difference, pyrite-chalcopyrite (0.1 V) and chalcopyrite-sphalerite (0.1 V). The results for sulphide mixtures in stage A are shown in Figure 4.6. With mixtures of low rest-potential difference ($\leq$ 0.1 V) no self-heating was observed; however, when mixtures of high rest-potential difference ($\geq$ 0.35 V) were formed self-heating was observed. The results for stage B showed a similar trend (Appendix, Figure A 3). Again, it appears that galvanic interaction between the sulphides influences self-heating.

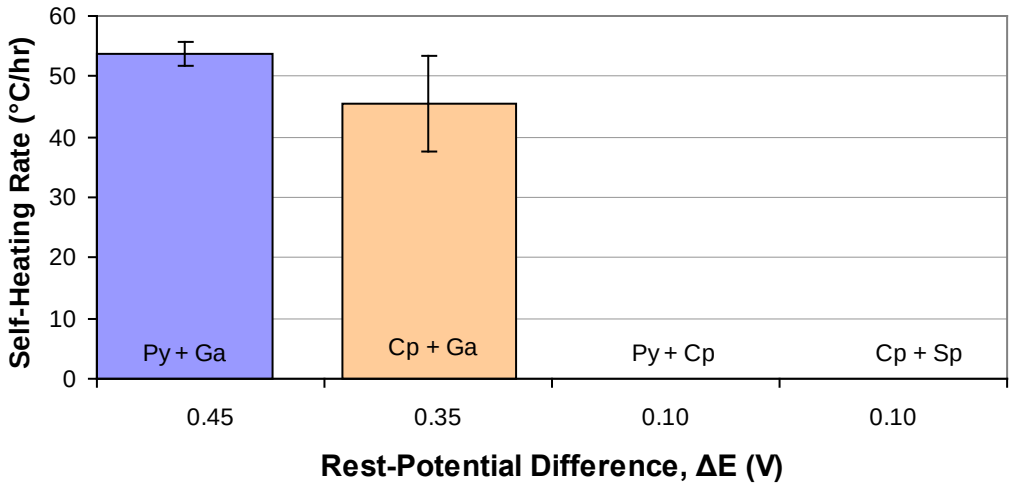

Figure 4.6: Stage A self-heating rate in non-pyrrhotite sulphide mixtures

The samples used in this section mainly comprised concentrates, which contain various minerals and may carry traces of the reagents used during mineral processing. There is a possibility that these 'contaminants' affect galvanic interaction. This prompted the 'purer' mineral samples work.

4.2.3. 'Purer' Sulphides Systems

The same experiments were run as in section 4.2.2 with one additional mixture, pyrite and sphalerite (Py-Sp) (rest-potential difference, 0.22V). The results are shown in Figure 4.7. Individual sulphides did not self-heat (see Appendix, Table A 3).

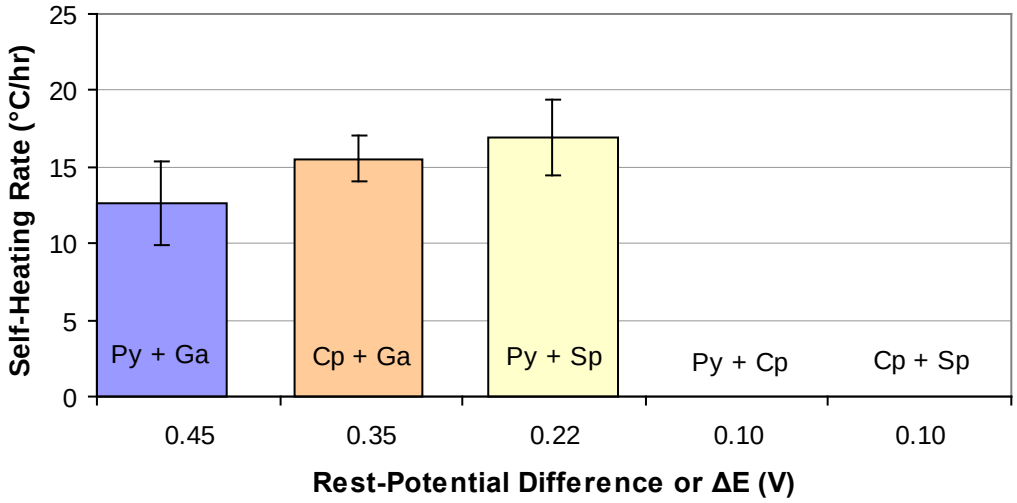

Figure 4.7: Stage A self-heating rate for 'purer' sulphide mixtures

The results were similar to those described with concentrates: mixtures of high rest-potential difference did self-heat. The heating rates for these systems were lower than in the case with concentrates that may have several origins (other contaminants, lower surface area). As a guide to the cut-off rest-potential difference, i.e., that dividing mixtures that self-heat from those that do not, based on the fact that self-heating occurred in the Py-Sp case (Figure 4.7), it appears to be ca. 0.2 V.

In both pyrrhotite and non-pyrrhotite systems, therefore, only mixtures with high rest-potential difference (> ca. 0.2 V) self-heated suggesting galvanic interaction. However, there was no control over particle size, which influences galvanic interaction through the surface area of mineral contact.

4.2.4. Controlled Particle Size Systems

For this section, the Py-Sp mixture was selected and monitored for self-heating response as a function of the particle size. Pyrite and sphalerite were separately

size reduced to produce four particle sizes: 80 % passing 825 µm, 340 µm, 70 µm and 25 µm.

The pyrite and sphalerite were first tested individually. Sphalerite did not self-heat on its own in stage A or B at any size (Appendix, Table A 4). Pyrite, however, heated in stage A for samples 80 % passing 25 µm and in stage B, for samples 80 % passing 70 µm and finer (Figure 4.8).

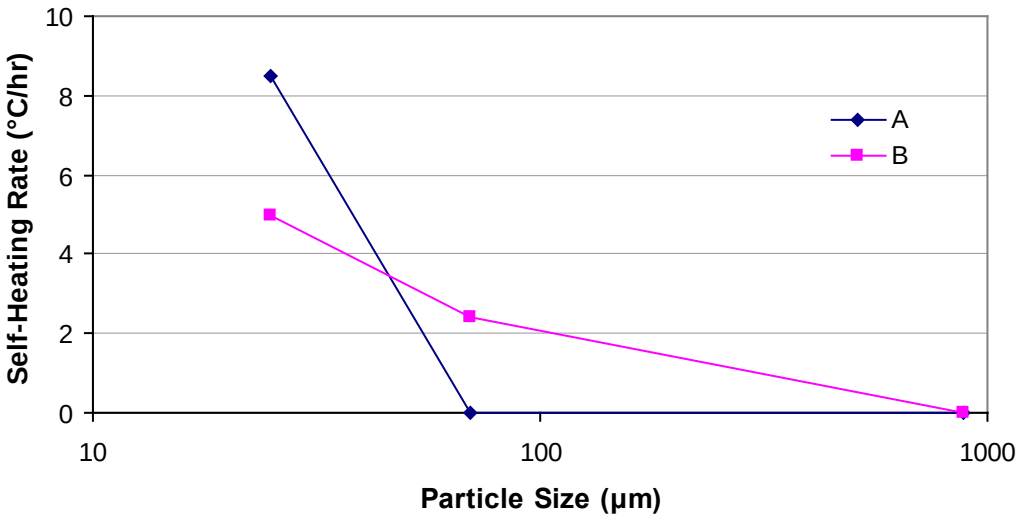

Figure 4.8: Self-heating rate of pyrite in stages A and B versus particle size

Mixtures of the same particle size were prepared and the results are in Figure 4.9. This shows that self-heating did occur in both stages A and B for the Py-Sp mixtures (as before) and increased markedly with decrease in particle size, greatly exceeding that for pyrite alone at the finest sizes (Figure 4.8). In other words, there was galvanic interaction that increased as surface area of contact increased.

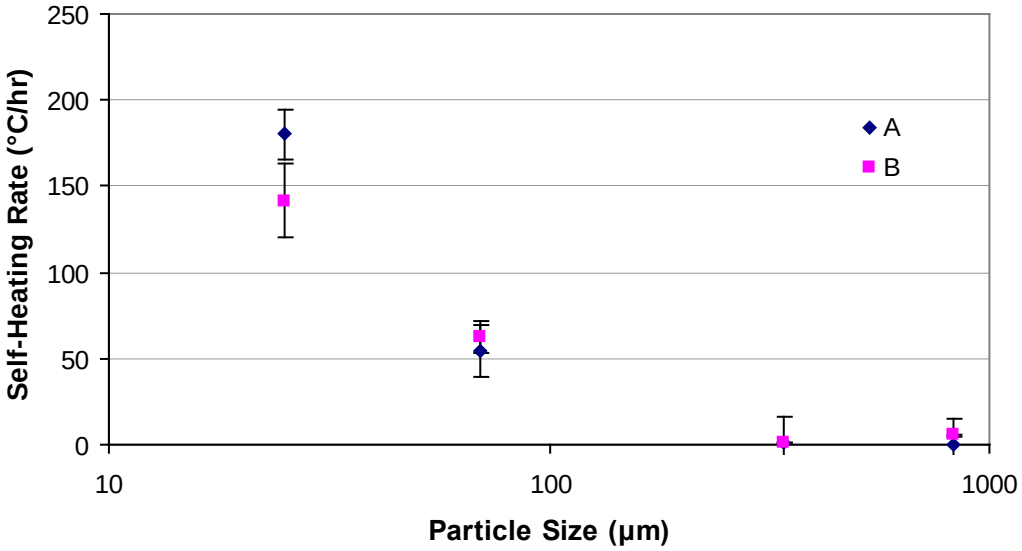

Figure 4.9: Self-heating rate in stages A and B for pyrite and sphalerite mixtures versus particle size

The tests used the same particle size for both Py and Sp. Two further tests were conducted mixing minerals of different size particle. In test 1, a sample was formed by combining the largest particle size of pyrite (80 % -825 µm) with the smallest sphalerite (80 % -25 µm); and in test 2, a sample was formed by combining the smallest pyrite (80 % -25 µm) with the largest sphalerite (80 % -825 µm). The results for both tests are in Figure 4.10. In test 1, while self-heating is observed, rates remain below 10 °C/hr. In contrast, in test 2 self-heating rates for both stages A and B are above 40 °C/hr. This means that the surface area of Py, the cathodic mineral, is more important in self-heating than that of the Sp, the anodic mineral. The 40 °C/hr SHR, note, is well above that for the same size Py on its own (Figure 4.8); in other words galvanic effects are still in evidence.

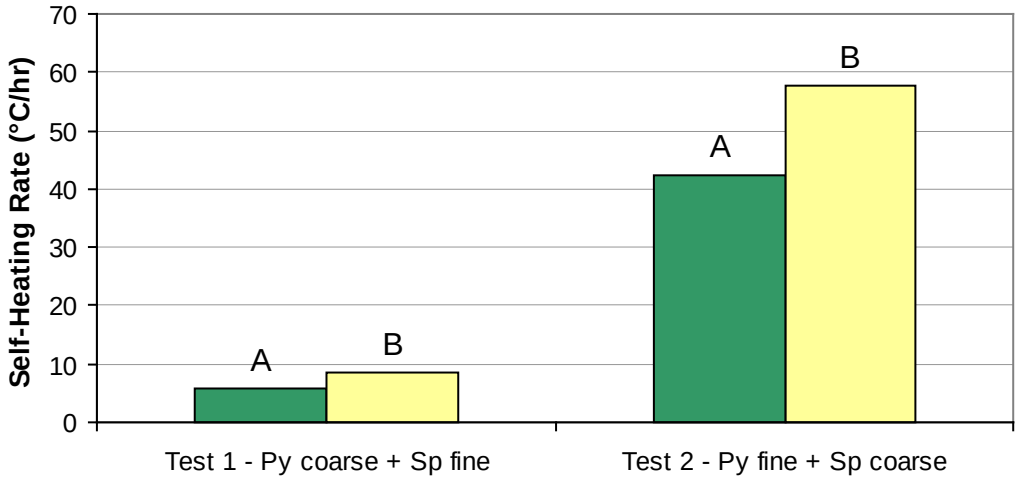

Figure 4.10: Self-heating rate in stages A and B for mixtures of pyrite and sphalerite of different particle size

The self-heating rate of stage A and stage B was plotted versus the surface area in Figure 4.11 and Figure 4.12, respectively. The start of the surface area data corresponds to the 80 % - 340 μm case. Since the particle size-surface area trends are different for the two minerals there are three trends shown: against Py, Sp and the weighted (50:50) average (the trend between the other two). In stage A (Figure 4.11), a direct proportionality between the surface area and the self-heating rate is suggested. In stage B (Figure 4.12) a similar trend to that in stage A is observed, although not quite as linear.

Taking the slope of self-heating rate vs. the average surface area (the centre trend line) in Figure 4.11 yields a specific rate per unit area for the material: for stage A this is $325 \frac{g \cdot {}^{\circ}C}{m^2 \cdot hr}$.

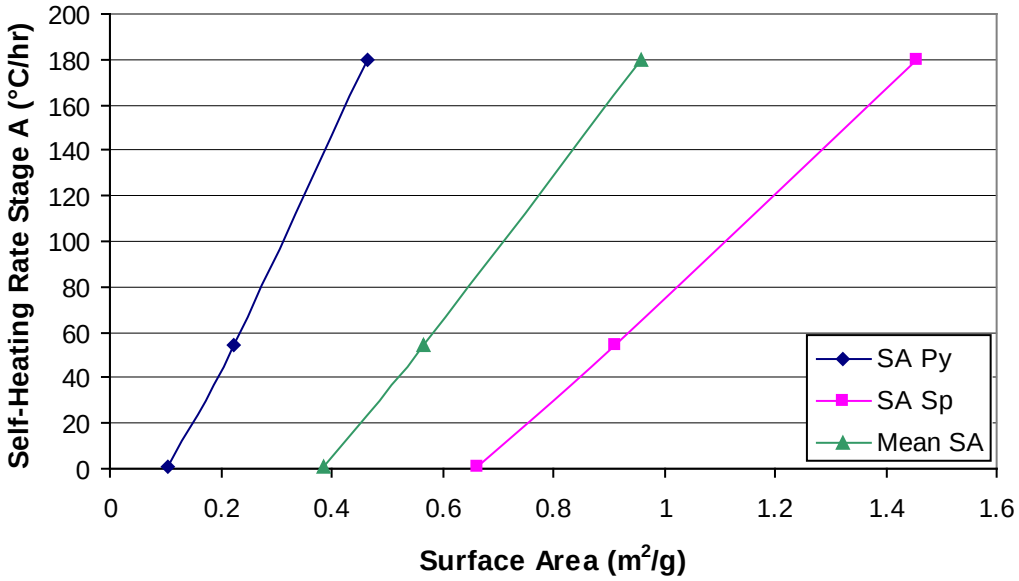

Figure 4.11: Stage A self-heating rate against the surface area of pyrite, sphalerite and the average of both

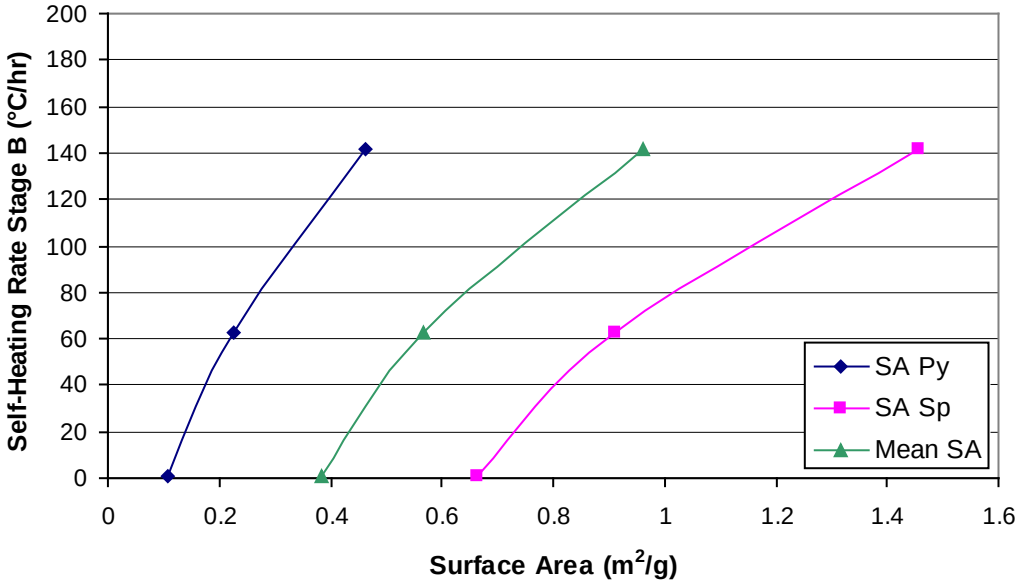

Figure 4.12: Stage B self-heating rate against the surface area of pyrite, sphalerite and the mean of both pyrite and sphalerite

4.3. Risk Assessment Charts

4.3.1. Pyrrhotite Systems

The risk assessment chart compares a sample's stage A and stage B self-heating capacity in relation to five risk zones. In Figure 4.13, the single mineral 25 % Py and 50 % Py samples, respectively, fall into zone 3 and zone 4. The single mineral 25 % Po sample falls into the potentially hazardous zone 5. Both mixtures, 25 % Py-25 % Po and 50 % Py-25 % Po, fall close together and further into zone 5 than Po alone.

The Py-Pn system is presented in Figure 4.14. As above, the 25 % Py and 50 % Py samples fall into zone 3 and 4, respectively. The single mineral 25 % Pn sample falls into zone 4 but the two Py-Pn mixtures move into the potentially hazardous zone 5.

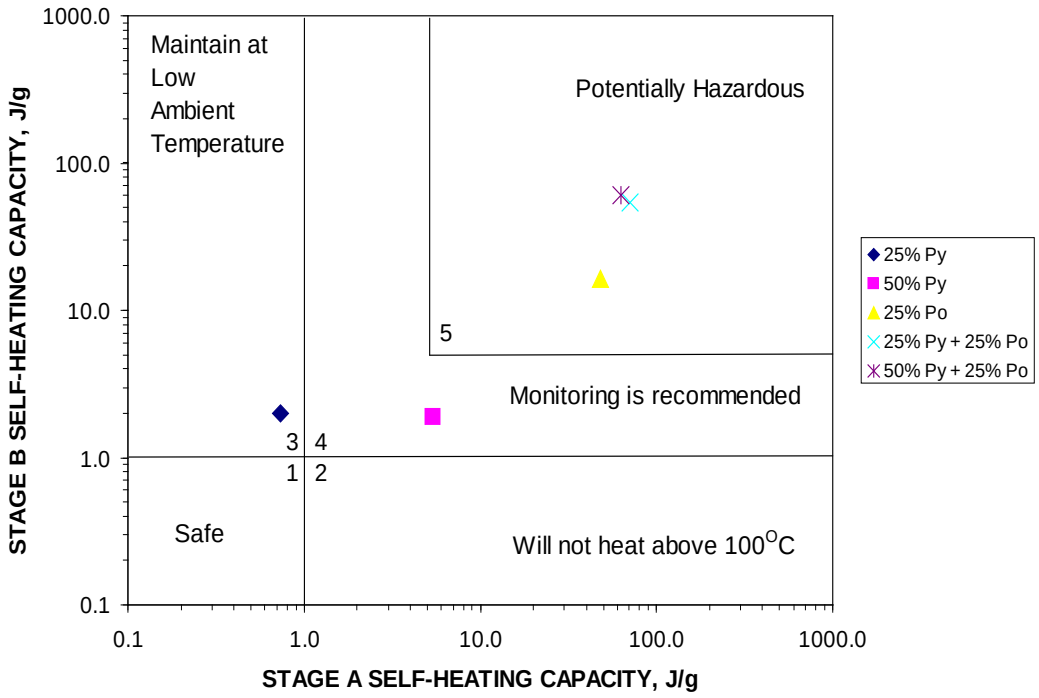

Figure 4.13: Risk assessment chart for pyrite-pyrrhotite systems

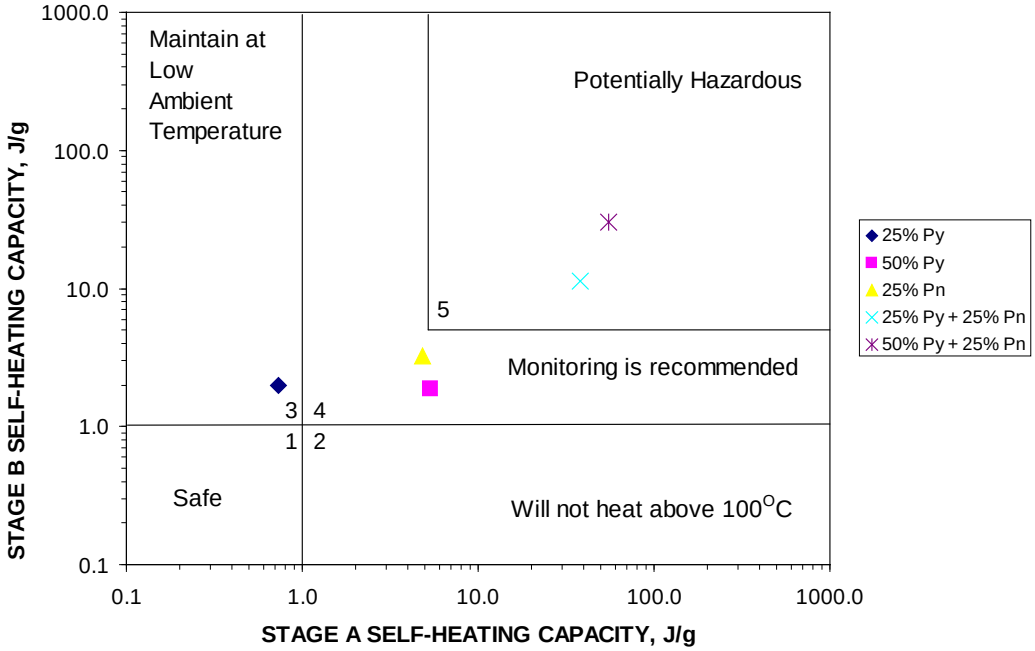

Figure 4.14: Risk assessment chart for pyrite-pentlandite systems

4.3.2. Non-Pyrrhotite Systems

The results for non-pyrrhotite systems are presented in Figure 4.15. The four sulphides tested individually and in mixtures of low rest-potential difference (pyrite-chalcopyrite and chalcopyrite-sphalerite) are found in zone 1. These are considered inactive. Sulphide mixtures with a high rest-potential difference, Py-Ga and Cp-Ga, became active systems, falling into zone 4 and 5, respectively.

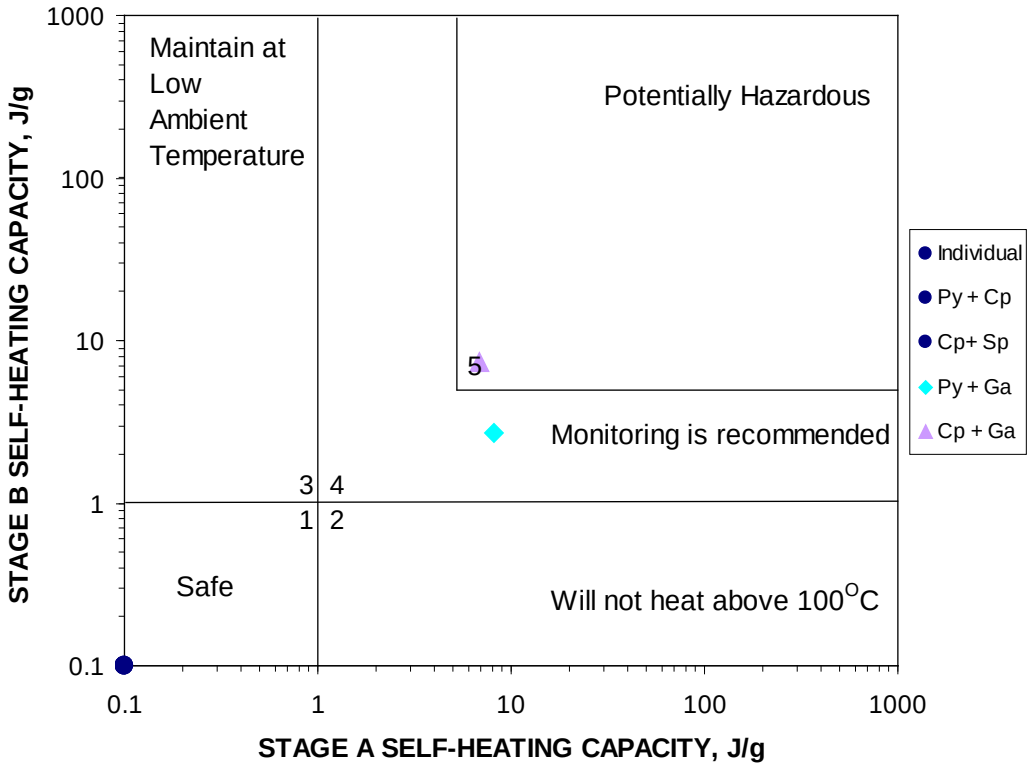

Figure 4.15: Risk assessment chart for non-pyrrhotite systems

4.3.3. 'Purer' Sulphides Systems

The results for these systems are presented in Figure 4.16. The four sulphides tested individually and the mixtures of low rest-potential difference again are found in zone 1. Sulphide mixtures with a high rest-potential difference became active systems, Py-Sp falling into zone 2, and Py-Ga and Cp-Ga falling into zone 4.

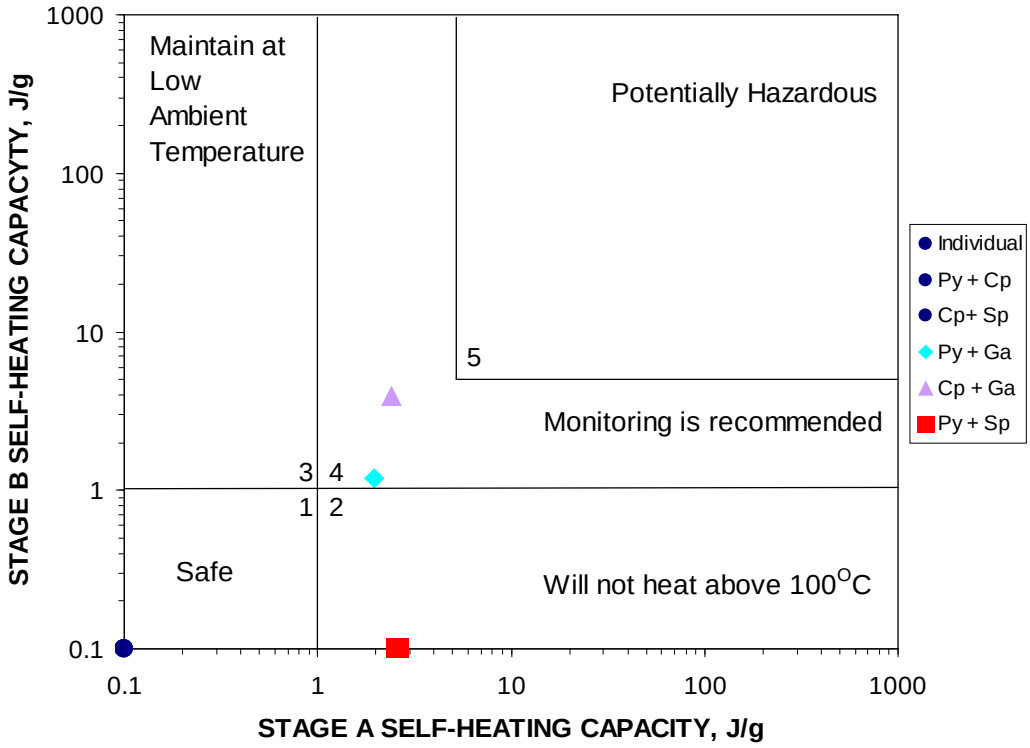

Figure 4.16: Risk assessment chart for 'purer' sulphide systems

4.3.4. Controlled Particle Size Systems

The data from these experiments are presented on the risk assessment chart in Figure 4.17. The two mixtures with largest particle sizes, 80 % -825 μm and 80 % -340 μm, remained in safe zone 1 while the two smaller particle size mixtures, 80 % -70 μm and 80 % -25 μm, moved into the potentially hazardous zone 5.

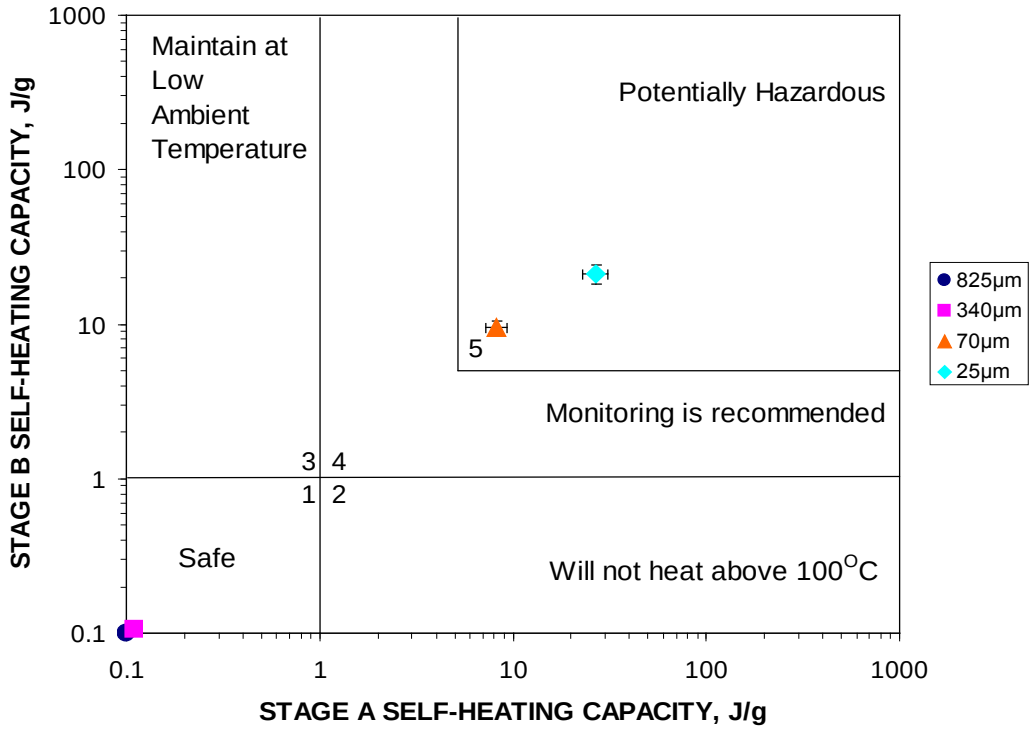

Figure 4.17: Risk assessment chart for pyrite and sphalerite mixtures of controlled particle size

To test whether it was fine particle size alone or as a component of galvanic interaction that was important, the self-heating capacities of pyrite alone at two different particle sizes were compared to a sample of pyrite mixed with coarse and fine sphalerite (Figure 4.18). For pyrite alone no heating was observed at 80 % -825 µm (zone 1). Some heating was seen in the 80 % -25 µm pyrite sample, moving it to zone 2. When coarse sphalerite (80 % -825 µm) is added to the 80% -25 µm pyrite sample the response registered in zone 5 and it moved further into zone 5 when the pyrite and sphalerite were both at a small particle size (80 % -25 µm). Thus fine particle size is acting primarily to increase galvanic interaction.

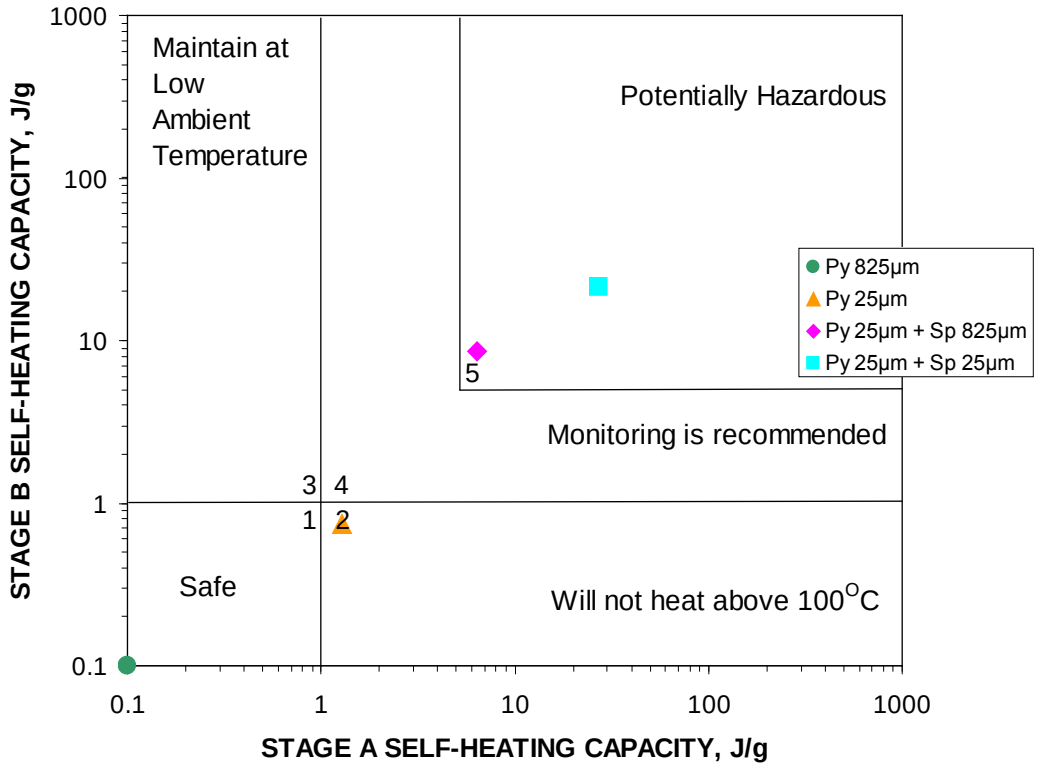

Figure 4.18: Risk assessment chart for pyrite alone compared to mixtures of pyrite and sphalerite

Chapter 5 Discussion

The discussion is separated into five sections, one for each system tested and a fifth section on galvanic interaction.

5.1. Pyrrhotite-containing Systems

The scale of the standard test (500 g) imposes problems in generating sufficient sample. This dictates the use of plant-derived samples such as concentrates. Thus, in common with all the systems tested, the three samples in the pyrrhotite-containing systems, pyrite, pentlandite and pyrrhotite, contained impurities (section 4.1.1). These impurities could affect the self-heating results. However, regardless of this possibility the self-heating rate was significantly greater for the Py-Po mixture than for both Py and Po alone; e.g. Figure 4.2, shows 10 °C/hr for 25 % Py and 320 °C/hr for 25 % Po, the sum of which was smaller than the self-heating rate of the mixed sulphides, 475 °C/hr for 25 % Py-25 % Po. This effect of the mixture over the individual samples is further emphasized in the risk assessment charts (Figure 4.13 and Figure 4.14). The difference was more pronounced with the Py-Pn mixture: the 25 % Pn sample fell into zone 4 of the risk assessment chart (Figure 4.14) but when mixed with pyrite, it moved into zone 5. The additional heating obtained with the Py-Po and Py-Pn combinations strongly suggests an origin in galvanic interaction between the sulphides. Given the presence of Py, the sulphide with the highest rest-potential of the common sulphides, in both systems adds to this conclusion.

From the literature, the rest-potentials for pyrite, pentlandite and pyrrhotite were estimated at 0.66 V, 0.35 V and 0.31 V, respectively (Table 2.2). Consequently, the rest-potential difference for the mixture Py-Po was 0.35 V and for Py-Pn 0.31 V. As a higher rest-potential difference means a larger driver for galvanic interaction (Rao and Finch, 1988), one might expect the Py-Po mixture to have higher self-heating rates than the Py-Pn mixture. The results reflect this both in stages A and B (Figure 4.2 to Figure 4.5). Despite the rest-potential values being

derived from literature, where sample origin can be a factor, this observation and interpretation prompted the subsequent work to assess the role of galvanic interaction in promoting self-heating and to estimate the magnitude of rest-potential difference ($\Delta E \sim 0.3$ V) required to effect self-heating.

5.2. Non-pyrrhotite Systems

Four common sulphides were chosen to test a range of rest-potential differences, again determined from literature values (Table 2.2). Since the selected sulphides do not typically self-heat, and this proved to be the case, if they became active on mixing it could be readily attributed to galvanic interaction, especially if the self-heating rate proved dependent on ΔE. Again mixtures corresponding to the higher rest-potential differences did self-heat (Figure 4.6). While the data are limited, $\Delta E > 0.3$ V appeared to correspond to a 'high' difference in rest-potential associated with self-heating and $\Delta E \leq 0.1$ V corresponded to a 'low' difference associated with no self-heating.

It was recognized that the galena (lead concentrate) sample contained an appreciable amount of pyrite (Table 4.2). The Py-Ga and Cp-Ga combinations that self-heated may reflect the presence of this pyrite which increased the actual proportion of high rest-potential mineral in the mixture. This point may be a factor in the risk assessment chart where the Cp-Ga mixture, which had a lower rest-potential difference than the Py-Ga mixture, is found in zone 5 (Figure 4.15). The Cp-Ga mixture in reality is Cp-Ga-Py and the behaviour of three-mineral mixture may have triggered the additional self-heating response.

5.3. 'Purer' Sulphide Systems

To partly address the sample impurity issue, testing was repeated using 'purer', although still not pure, sulphides.

The same mixtures were formed as in the non-pyrrhotite system (i.e., section 5.2) with the addition of another high rest-potential difference combination (Py-Sp). The results for self-heating rate versus rest-potential difference (Figure 4.7) were the same as for the non-pyrrhotite system (Figure 4.6) but overall, the self-heating rate was lower for these 'purer' sulphide samples. This can be observed in the risk assessment chart, all points moving closer to zone 1 (Figure 4.16). With the addition of the Py-Sp mixture, the results showed that the rest-potential difference prompting self-heating corresponded to $\Delta E > 0.2$ V as opposed to the $\Delta E > 0.3$ V before. The low rest-potential difference cut-off remained the same at $\Delta E \leq 0.1$ V.

It was important to note that in this system and the previous non-pyrrhotite system particle size was not controlled. One of the two main factors affecting galvanic interaction (section 2.5) is the particle size or relative surface area of contacting sulphides

5.4. Controlled Particle Size Systems

A Py-Sp mixture, a common combination, was chosen for this work. The sulphides were individually size reduced and mixed. Mixtures of Py-Sp of the same particle size (80 % passing size) showed increasing self-heating rates with decreasing particle size. On the risk assessment chart (Figure 4.17), as particle size decreased the samples moved progressively deeper into zone 5. The decrease in particle size is associated with an increase in surface area: the larger the surface area, the more contact between pyrite and sphalerite is created, encouraging electron flow and thus galvanic interaction.

Testing the effect of surface area, the relationship with self-heating rate in stage A was approximately linear for this 1:1 weight ratio. This was not the case for stage B (at 140 °C), which may reflect the absence of the water required for galvanic interaction. Previous researchers have noted that the products formed during the weathering stage A serve as fuel for stage B (Rosenblum and Spira, 1995), but

this may not result in the same dependence on surface area. It is possible that at a certain particle size, the products formed in stage A might level off and this would explain why the trends in stage B (Figure 4.12) increase more slowly than in stage A (Figure 4.11).

When varying the particle size of the individual components in Py-Sp mixture (Figure 4.10) the self-heating rate remained below 10 °C/hr for Test 1 (Py coarse-Sp fine) and above 40 °C/hr for Test 2 (Py fine-Sp coarse). Decreasing the particle size of pyrite with sphalerite held constant at 'coarse' generated a large increase in the self-heating rate, higher than fine pyrite alone as seen in Figure 4.8. In a galvanic cell, pyrite would be the cathode and sphalerite the anode. The significant increase in self-heating rate as the size of the cathodic pyrite is reduced emphasizes the importance of the reduction step in the galvanic interaction leading to self-heating. It seems the reduction step is rate-limiting. The large surface area of pyrite allowed electrons to be accepted more easily by electron acceptors such as ferric species and oxygen. The importance of the cathode surface area relative to the anode surface area in promoting galvanic interaction has been noted by others (Yelloji Rao and Natarajan, 1989; Kwong et al., 2003). In regard to the relationship with surface area, following the above observation, it may be that only the surface area of Py needs be considered in Figure 4.11 and Figure 4.12.

In the risk assessment chart (Figure 4.18), pyrite alone at its largest particle size (80 % -825 μm) fell into zone 1 and at its smallest particle size (80 % -25 μm) fell into zone 2. As fine pyrite was mixed with coarse sphalerite the result moved to zone 5 and as fine pyrite was mixed with fine sphalerite the result moved further into zone 5. This shows galvanic interaction is at play controlled both by the difference in rest-potential and surface area of the cathodic pyrite.

5.5. Galvanic Interaction and Self-Heating

In order for galvanic interaction, an electrolyte medium is required. The moisture present in stage A can serve as the electrolyte, and it is notable that self-heating at low temperatures only occurs in the presence of moisture. This supports the suggestion that the self-heating mechanism has a component of electrochemistry (Kirshenbaum, 1968; Ninteman, 1978; Rosenblum and Spira, 1995; Wang, 2007).

According to the results, a high rest-potential difference (ΔE) triggering self-heating is approximately 0.2 V and a low ΔE where self-heating does not occur is about 0.1 V. Interestingly, any $\Delta E > 0.1$ V will likely cause galvanic corrosion and any potential $\leq$ 0.1 V will not (Australian Stainless Steel Development Association, 2008).

The question now is to connect to self-heating. The approach is to consider the H_2S hypothesis: building on this concept proposed by Somot and Finch (2010). There may be alternate pathways for H_2S formation than the one they suggested, Equation 2.26. Harmer et al. (2006) proposed Equation 2.50, in which a polysulphide species reacts with ferrous iron in an acidic environment to produce H_2S. Polysulphides can be expected on most sulphide surfaces due to some superficial oxidation (Rao and Leja, 2004). In addition to H_2S, Equation 2.50 yields ferric ions. Any subsequent reduction of ferric iron (Equation 2.49) would form an oxidation-reduction cycle in which the formation of H_2S would be promoted. This opens an interesting possibility relevant to the present findings.

There are several ways in which ferric iron can be reduced to ferrous iron. It is likely that the sulphide mineral present in the system will reduce ferric iron (Steger, 1979). It is also a possibility that ferric is reduced to ferrous as a cathodic reaction in galvanic interaction. In a galvanic cell, ferric iron (Equation 2.49) might even be the preferred electron acceptor over oxygen (Equation 2.48) because it gives a higher rate of reaction (Moses et al., 1987). The reaction loop

favouring H_2S formation proposed by Harmer et al. (2006) appears to be at play here in promoting self-heating.

The self-heating of sulphides is associated with oxidation (Kirshenbaum, 1968; Rosenblum and Spira, 1981). In an electrochemical model oxidation is coupled with a reduction step. In that case although oxidation is the exothermic reaction it is dependent on the reduction step which may be rate-limiting. From the evidence here, self-heating of sulphide appears to involve this oxidation-reduction mechanism opening a role for galvanic interaction as an explanation for self-heating of some sulphide mixtures.

Chapter 6 Conclusions and Recommendations

6.1. Conclusions

Sulphide mixtures with pyrrhotite showed that even though pyrrhotite and pentlandite heat on their own, the addition of pyrite can significantly increase self-heating.

In the non-pyrrhotite systems, individual samples of pyrite, chalcopyrite, sphalerite and galena did not self-heat. When mixed, combinations with high rest-potential difference ($\Delta E > 0.2$ V) self-heated and combinations with low rest-potential difference ($\Delta E \leq 0.1$ V) did not.

Inactive coarse pyrite did become active when finely ground. Nevertheless when mixed with sphalerite self-heating increased. It was shown that the particle size (surface area) of the pyrite in the mixture was more important than the particle size of the sphalerite.

The observations indicate self-heating in the mixtures is through galvanic interaction driven by the magnitude of the rest-potential difference and surface area of the cathodic mineral (pyrite in the cases studied). Based on the H_2S hypothesis it is postulated that a cycle is formed with ferrous iron reacting with polysulphide to produce H_2S and ferric ions which then act as the electron acceptor in the galvanic interaction and are reduced back to ferrous.

6.2. Recommendations

To try to determine the critical relative surface area of pyrite which triggers self-heating by experimenting with varying particle size and amount of pyrite in mixtures with sphalerite. This critical level could be a guide for use in determining the hazard associated with transport and storage of non-pyrrhotite materials.

To examine cases where samples of non-pyrrhotite containing materials self-heat for presence of pyrite and pyrite surface area to cross reference to the above lab study.

To determine if moisture control provides an effective way to mitigate self-heating given that moisture is the common component in self-heating materials with otherwise very divergent mineralogy.

References

Abriatis, P.K., Pattrick, R.A.D., Kelsall, G.H., Vaughan, D.J. (2004). Acid Leaching and Dissolution of Major Sulphide Ore Minerals. Process and Galvanic Effects in Complex Systems. Mineralogical Magazine 68:343-351.

Adam, K., Natarajan, K.A., Iwasaki, I. (1984). Grinding media wear and its effect on the flotation of sulfide minerals. International Journal of Mineral Processing 12:39-54

Australian Stainless Steel Development Association. (2008) Galvanic/Dissimilar Metal Corrosion. Retrieved 04-15-2009 from: http://l-36.com/galv.pdf

Belzile, N., Chen, Y.W., Cai, M.F., Li, Y. (2004). A review on pyrrhotite oxidation. Journal of Geochemical Exploration 84:65-76.

Bowes, P.C. (1954). Spontaneous Heating and Ignition in Iron Pyrites. The Industrial Chemist 12-14.

Chen, X.D. (2001). Self-heating behaviour of low moisture content particles-modelling the basket-heating of solid particles and some aspects of the cross over behaviour using milk powder as an example. The ANZIAM Journal 43:165-181.

Chen, Y.W., Li, Y., Cai, M.F., Belzile, N., Dang, Z. (2006). Preventing oxidation of iron sulfide minerals by polyethylene polyamines. Minerals Engineering 19:19-27.

Cruz, R., Gonzalez, I., Monroy, M. (2005). Electrochemical Characterization of Pyrrhotite Reactivity Under Simulated Weathering Conditions. Applied Geochemistry 20:109-121.

Das, A., Mishra, A.K. (1996). Role of Thiobacillus Ferrooxidans and Sulphur (sulphide)-Dependent Ferric-ion-reducing Activity in the Oxidation of Sulphide Minerals. Applied Microbiology and Biotechnology 45:377-382.

Dixon, D.G., Mayne, D.D., and Baxter, K.G. (2007). Galvanox-A Novel Galvanically-Assisted Atmospheric Leaching Technology for Copper Concentrates. Cu 2007. The John E. Dutrizac International Symposium on Copper Hydrometallurgy IV(1), 191-207.

Farnsworth, D.J.M. (1977). Introduction to and Background of Sulphide Fires in Pillar Mining at the Sullivan Mines. CIM Bulletin 70:65-71.

Finch, J., Rao, S.R., Nesset, J.E. (2006). Iron control in mineral processing. Iron Control Technologies, Proceedings of the International Symposium on Iron Control in Hydrometallurgy, 3rd, Montreal, QC, Canada, Oct 1-4.

Good, B.H. (1977). The Oxidation of Sulphide Minerals in the Sullivan Mine. CIM Bulletin 70:83-88.

Gottschalk, V. (1912). Oxidation of Sulfides II. Economic geology and the bulletin of the Society of Economic Geologists 7:15.

Gunsinger, M.R., Ptacek, C.J., Blowes, D.W., Jambor, J.L. (2006). Evaluation of Long-Term Sulfide Oxidation Processes within Pyrrhotite-Rich Tailings, Lynn Lake, Manitoba. Journal of Contaminant Hydrology 83:149-170.

Habashi, F. (1966). The mechanism of oxidation of sulfide ores in nature. Economic Geology 61:587-591.

Harmer, S.L., Thomas, J.E., Fornasiero, D., Gerson, A.R. (2006). The Evolution of Surface Layers Formed During Chalcopyrite Leaching. Geochimica Cosmochimica Acta 70:4392-4402.

Harrington, D., Pickard, B.O., Wolfin, H.M. (1923). Metal Mine Fires. Department of the Interior Technical Paper 314.

Headley, G.S., Bloomer, T.O., Glennie, J.A. (1977). Hot muck mining methods. CIM Bulletin 70:72-78.

Janzen, M.P., Nicholson, R.V., Sharer, J.M. (2000). Pyrrhotite Reaction Kinetics: Reaction Rates for Oxidation by Oxygen, Ferric Iron and for Nonoxidative Dissolution. Geochimica Cosmochimica Acta 64:1511-1522.

Kirshenbaum, N.W. (1968). Transport and Handling of Sulphide Concentrates: Problems and Possible Improvements, 2nd edn. Technomic Publishing Company, Inc., Stamford, Connecticut.

Klassen, V.I., Mokrousov, V.A. (1963). An Introduction to the Theory of Flotation. Butterworths, London.

Kocabag, D. (1985). The effect of grinding media and galvanic interactions upon the flotation of sulfide minerals. Complex Sulfides, Proc Symp 55.

Konishi, Y., Kubo, H., Asai, S. (1992). Bioleaching of zinc sulfide concentrate by Thiobacillus ferrooxidans. Biotechnology and Bioengineering 39:66-74.

Kwong, Y.T.J., Swerhone, G.W., Lawrence, J.R. (2003). Galvanic Sulphide Oxidation as a Metal-Leaching Mechanism and its Environmental Implications. Geochemistry: Exploration, Environment, Analysis 3:337-343.

Lukaszewski, G. M. (1973). Sulphides in Underground Mine Filling Operations. Jubilee Symposium on Mine Filling Mt Isa. 87-96.

Mehta, A.P., Murr, L.E. (1983). Fundamental Studies of the Contribution of Galvanic Interaction to Acid-Bacterial Leaching of Mixed Metal Sulphides. Hydrometallurgy 9:235-256.

Meng, T., Wu, C., Wang, P. (1993). Study on Spontaneous Combustion of Sulphide Ores. In: Proceedings of the 6th US Mine Ventilation Symposium.

Mielke, R.E., Pace, D.L., Porter, T., Southam, G. (2003). A critical stage in the formation of acid mine drainage: Colonization of pyrite by Acidithiobacillus ferrooxidans under pH-neutral conditions. Geobiology 1:81-90.

Moses, C.O., Nordstrom, D.K., Herman, J.S., Mills, A.L. (1987). Aqueous pyrite oxidation by dissolved oxygen and by ferric iron. Geochimica et Cosmochimica Acta 51:1561-1571.

Natarajan, K.A. (1992). Electrobioleaching of base metal sulfides. Metallurgical and Materials Transaction B 23:5-11.

Ninteman, D.J.(1978). Spontaneous Oxidation and Combustion of Sulfide Ores in Underground Mines: A Literature Survey. United States Department of the Interior Bureau of Mines Information Circular 8775.

Noranda Technology Centre. (1975). Brunswick Mine, unpublished report.

Nordstrom, D.K., Southam, G. (1997). Geomicrobiology of sulfide mineral oxidation. Reviews in mineralogy 35:361-390.

Norris, P.R., Parrott, L. (1985). High Temperature, Mineral Concentrate Dissolution with Sulfolobus. Fundamental and Applied Biohydrometallurgy. Elsevier, Amsterdam, pp 355-365.

O'Brien, M.M., Banks, H.R. (1926). The Sullivan Mine and Concentrator. Bulletin of Canadian Institute of Mining and Metallurgy 126:1214-1235.

Orlova, T. (1988). Mechanism of oxidative dissolution of sulfides. Zhurnal prikladno-¡ khimii 61:2172.

Pankratz, L.(1984) Thermodynamic properties of halides.

Rao, S.R., Finch, J.A. (1988). Galvanic Interaction Studies on Sulphide Minerals. Canadian Metallurgical Quaterly 27:253-259.

Rao, S.R., Labonte, G., Finch, J.A. (1992). Electrochemistry in the Plant. Innovations in Flotation Technology. Kluwer Academic Publishers, Netherlands, pp 57-100.

Rao, S.R., Leja, J. (2004). Surface Chemistry of Froth Flotation. Kluwer Academic/Plenum Publishers, New York.

Reimers, G.W., Hjelmstad, K.E. (1987). Analysis of the Oxidation of Chalcopyrite, Chalcocite, Galena, Pyrrhotite, Marcasite, and Arsenopyrite. 9118. United States Department of the Interior Bureau of Mines.

Rosenblum, F., Spira, P. (1981). Self-Heating of Sulphides. 34-49. CIM. The Thirteenth Annual Meeting of the Canadian Mineral Processors.

Rosenblum, F., Spira, P. (1995). Evaluation of Hazard from Self-Heating of Sulphide Rock. CIM Bulletin 88:44-49.

Rosenblum, F., Nesset, J., Spira, P. (2001). Evaluation and Control of Self-Heating in Sulphide Concentrates. CIM Bulletin 94:92-99.

Schippers, A., Kock, D., Schwartz, M., Böttcher, M.E., Vogel, H., Hagger, M. (2007). Geomicrobiological and geochemical investigation of a pyrrhotite-containing mine waste tailings dam near Selebi-Phikwe in Botswana. Journal of Geochemical Exploration 92:151-158.

Schippers, A., Jozsa, P.G., Sand, W., Kovacs, Z.M., Jelea, M. (2000). Microbiological Pyrite Oxidation in a Mine Tailings Heap and Its Relevance to the Death of Vegetation. Geomicrobiology Journal 17:151-162.

Shaw, S.S. (1998). Mineralogical study of base metal tailings with various sulfide contents, oxidized in laboratory columns and field lysimeters. Environmental Geology 33:209.

Somot, S., Finch, J.A. (2006). High Self-Heating Rate of Pyrrhotite-Rich Materials-H_2S as A Fuel? 38th Annual Meeting of the Canadian Mineral Processors. 83-92.

Somot, S., Finch, J.A. (2010). Possible role of hydrogen sulphide gas in self-heating of pyrrhotite-rich materials. Minerals Engineering 23:104-110.

Stachulak, J.S. (1994). Inco's Design and Protection Against Underground Fires. CIM Bulletin 87:58-63.

Stachulak, J.S. (1990). Computerized Fire Monitoring, Criteria, Techniques and Experience at Inco Limited. CIM Bulletin 83:59-67.

Steger, H.F. (1979). Oxidation of sulphide minerals: VI Ferrous and ferric iron in the water-soluble oxidation products of iron sulphide minerals. Talanta 26:455-460.

Steger, H.F. (1982). Oxidation of sulfide minerals: VII. Effect of temperature and relative humidity on the oxidation of pyrrhotite. Chemical Geology 35:281-295.

Steger, H,F,, Desjardins, L.E. (1978). Oxidation of Sulfide Minerals, 4.Pyrite, Chalcopyrite and Pyrrhotite. Chemical Geology 23:225-237.

Steger, H.F., Desjardins, L.E. (1980). Oxidation of sulfide minerals; V, Galena, sphalerite and chalcocite. Can Mineral 18:365-372.

Thomas, J.E., Skinner, W.M., Smart, R.S. (2001). A mechanism to explain sudden changes in rates and products for pyrrhotite dissolution in acid solution. Geochimica et Cosmochimica Acta 65:1-12.

Tributsch, H. Gerischer, H. (1976). The Oxidation and Self-Heating of Metal Sulphides as an Electrochemical Phenomenon. Journal of Chemistry and Biotechnology 26:747-761.

United Nations. Manual of Tests and Criteria. PART III - Classification Procedures, Test Methods and Criteria Relating to Calss 3, Class 4, Division 5.1 and Class 9. 2008.

United Nations. Recommendations on the Transport of Dangerous Goods Model Regulations. Twelfth Revised Edition. 2010.

Vanyukov, A. (1979). Hydrothermal oxidation of pyrrhotites. Izvestiya Vysshikh Uchebnykh Zavedenii, Tsvetnaya Metallurgiya28.

Wang, X., Rosenblum, F., Nesset, J.E., Somot, S., and Finch, J.A. (2009). Oxidation, Weight Gain and Self-Heating of Sulphides. Presented at the 41st Annual Meeting of the Canadian Mineral Processors. 63-77.

Wang, X., (2007). Exploring Conditions Leading to Self-Heating of Pyrrhotite-Rich Materials. Masters Thesis. McGill University.

Wegener, Schlieper. (1977). Research into the Spontaneous Combustion of Sulphide Lead, Copper, and Zinc concentrates. Laboratory 4.11, Diary 4-3602/1977 I. Bundesanstalt Fur Materialprufung (BAM).

Wong, W. (2005) Self-Heating of Sulphides. p. 59. Summer Project Report. McGill University.

Wu, C. (1995). Fault Tree Analysis of Spontaneous Combustion of Sulphide Ores and its Risk Assessment. Journal of Central South University of Technology 2:77-80.

Wu, C., Li, Z. (2005). A Simple Method for Predicting the Spontaneous Combustion Potential of Sulphide Ores at Ambient Temperature. Mining Technology (Transactions of the Institution of Mining and Metallurgy, Section A) 114:125-128.

Wu, C., Li, Z.J., Zhou, B., Wang, P.L., Li, M.N. (2001). Investigation of Chemical Suppressants for Inactivation of Sulfide Ores. Journal of Central South University of Technology 8:180-184.

Yelloji Rao, M.K., Natarajan, K.A. (1989). Electrochemical effects of mineral-mineral interactions on the flotation of chalcopyrite and sphalerite. International Journal of Mineral Processing 27:279-293.

Appendix

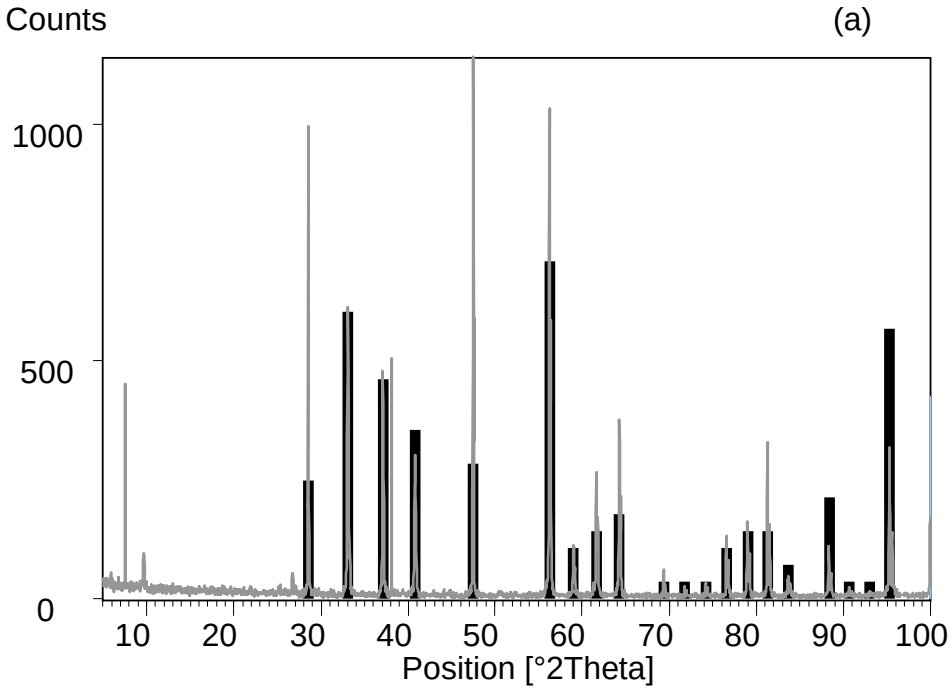
Counts
(a)
1000
500
0
10
20
30
40
50
60
70
80
90
100
Position [°2Theta]

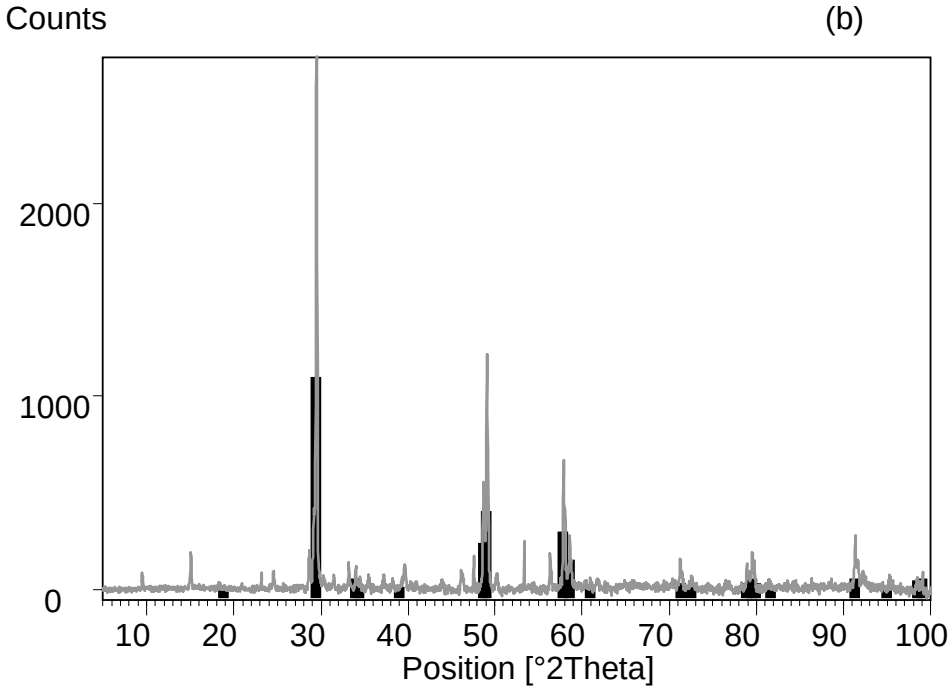
Counts
(b)
2000
1000
0
10
20
30
40
50
60
70
80
90
100
Position [°2Theta]

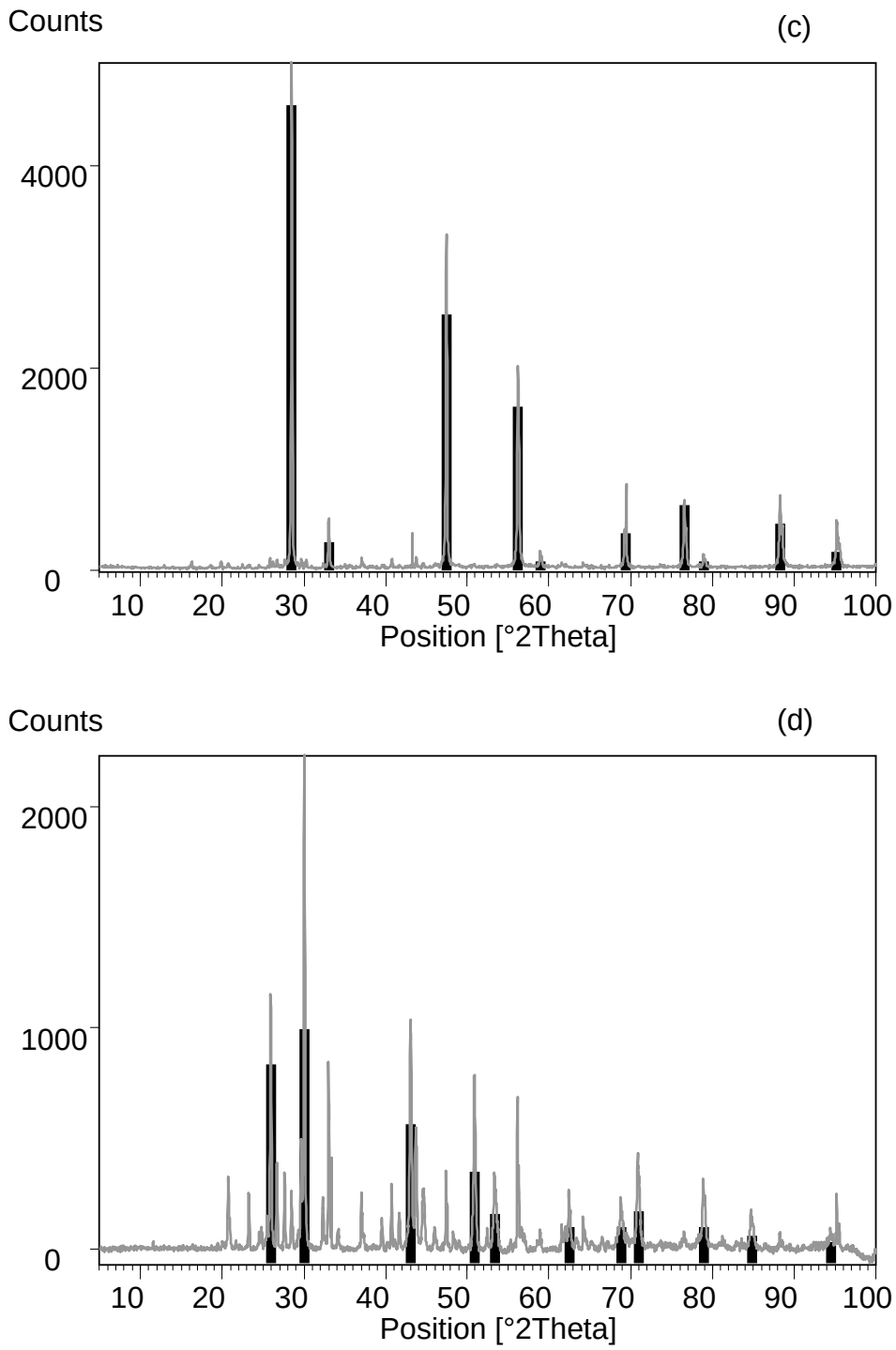

Figure A 1: X-ray diffraction patterns for non-pyrrhotite systems (a) pyrite (b) chalcopyrite, (c) sphalerite and (d) galena

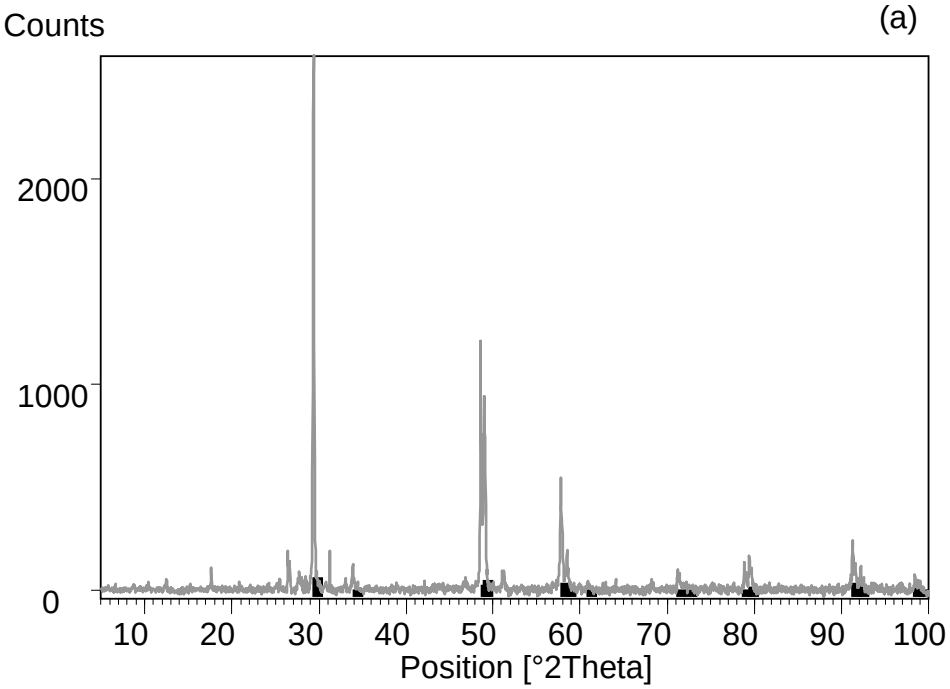
Counts
(a)
2000
1000
0
10
20
30
40
50
60
70
80
90
100
Position [°2Theta]

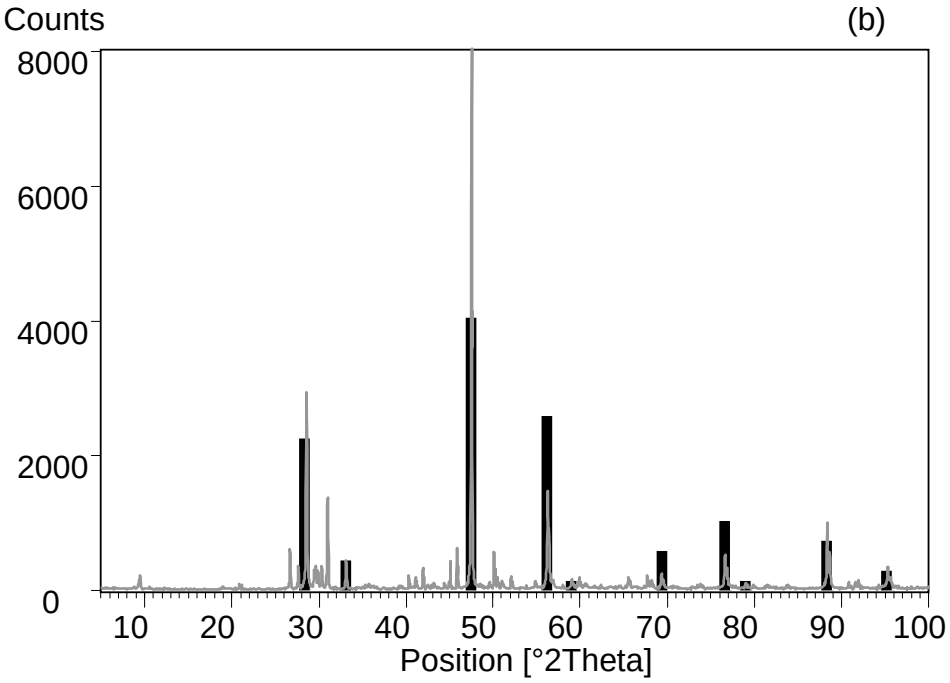
Counts
(b)
8000
6000
4000
2000
0
10
20
30
40
50
60
70
80
90
100
Position [°2Theta]

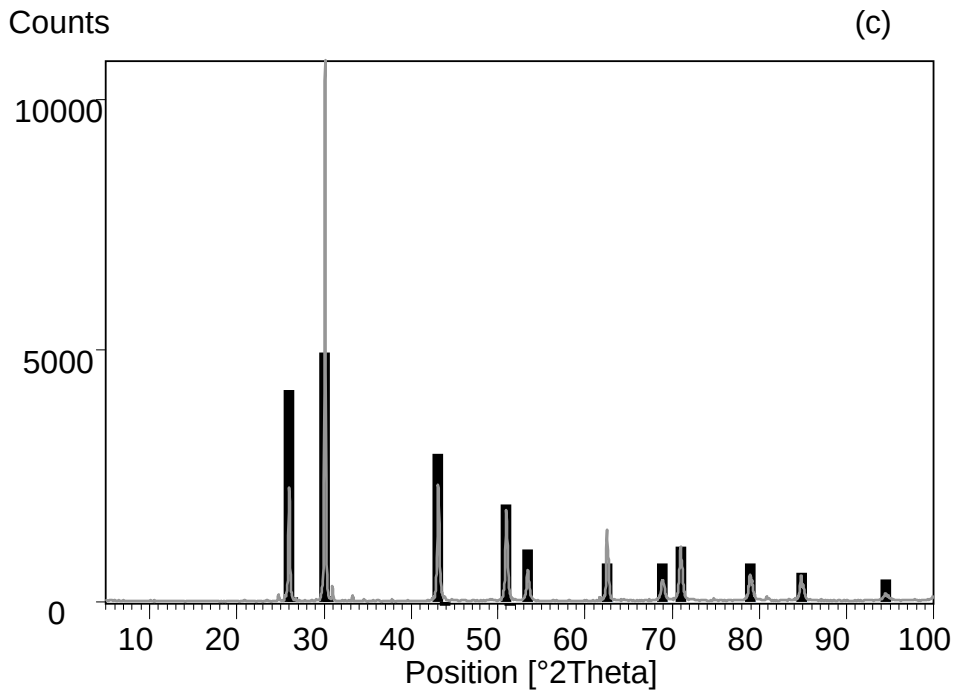

Figure A 2: X-ray diffraction patterns for 'purer' sulphide systems (a) chalcopyrite, (b) sphalerite and (c) galena

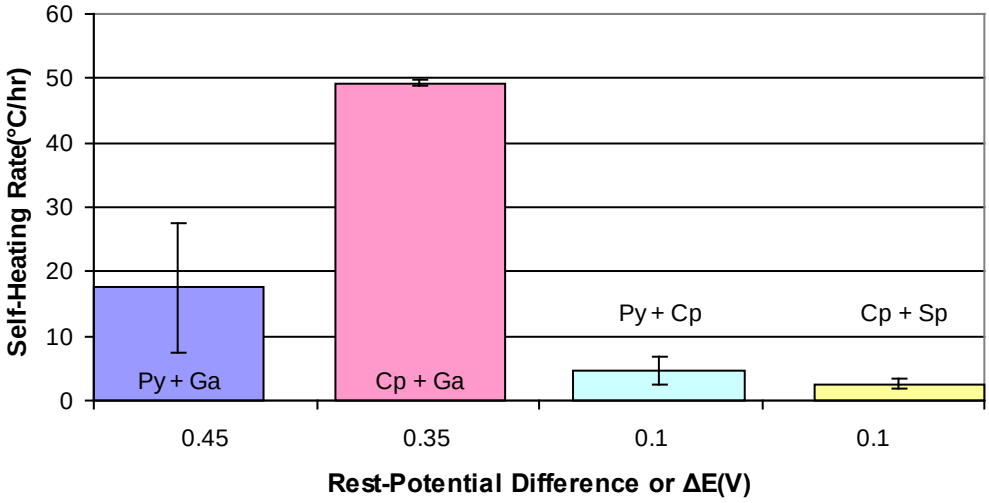

Figure A 3: Stage B: Self-heating rate in non-pyrrhotite sulphide mixtures

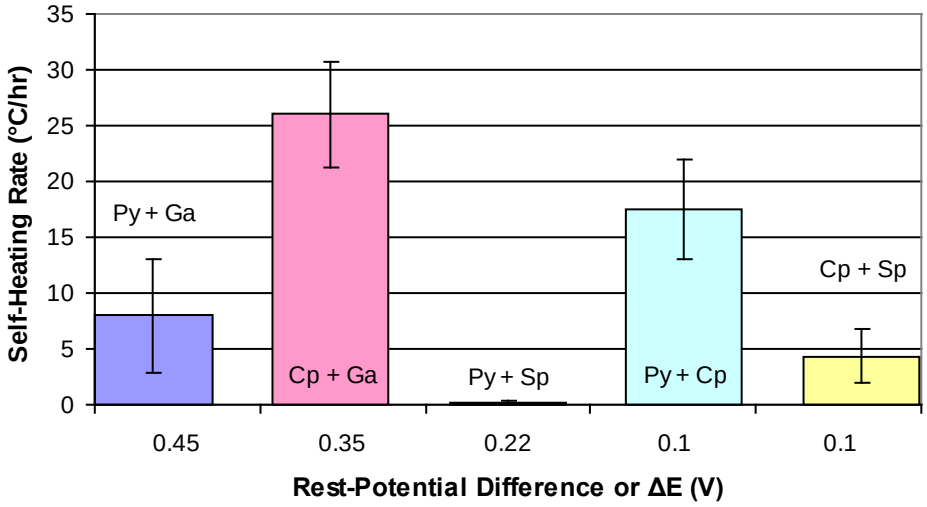

Figure A 4: Stage B: Self-heating rate for 'purer' sulphide mixtures

Table A 1: Pyrrhotite systems, self-heating rates (SHRs) and self-heating capacities (SHCs)

	SHR (°C/hr)		SHC (J/g)	
Sample	**A**	**B**	**A**	**B**
25% Py	4.90	13.3	0.735	2.00
50% Py	35.9	12.6	5.39	1.89
25% Po	321	109	48.1	16.3
25% Ni	32.4	21.8	4.86	3.27
25% Py + 25% Po	475	357	71.2	53.6
25% Py + 25% Ni	254	75.2	38.2	11.3
50% Py + 25% Po	420	400	63.0	60.0
50% Py + 25% Ni	369	202	55.4	30.3

Table A 2: Non-pyrrhotite systems, SHRs and SHCs

	SHR (°C/hr)		SHC (J/g)	
Sample	**A**	**B**	**A**	**B**
50% Py	0.00	1.70	0.00	0.255
50% Cp	0.00	1.00	0.00	0.150
50% Sp	0.00	1.90	0.00	0.285
50% Ga	0.00	2.00	0.00	0.300
50% Py + 50% Ga	53.7	17.5	8.06	2.63
50% Cp + 50% Ga	45.5	49.3	6.83	7.40
50% Py + 50% Cp	0.00	4.67	0.00	0.701
50% Cp + 50% Sp	0.00	2.90	0.00	0.435

Table A 3: 'Purer' sulphide systems, SHRs and SHCs

	SHR (°C/hr)		SHC (J/g)	
Sample	**A**	**B**	**A**	**B**
50% Py	0.00	1.70	0.000	0.225
50% Cp	0.00	23.8	0.00	3.57
50% Sp	0.00	0.00	0.00	0.00
50% Ga	0.00	0.60	0.00	0.09
50% Py + 50% Ga	12.6	8.00	1.89	1.20
50% Cp + 50% Ga	15.5	26.0	2.33	3.90
50% Py + 50% Sp	16.9	0.20	2.54	0.03
50% Py + 50% Cp	0.00	17.5	0.00	2.63
50% Cp + 50% Sp	0.00	4.30	0.00	0.645

Table A 4: Controlled particle size systems, SHRs and SHCs

	SHR (°C/hr)		SHC (J/g)	
Sample	**A**	**B**	**A**	**B**
50% Py 825 µm	0.00	0.00	0.00	0.00
50% Py 70 µm	0.00	2.40	0.00	0.360
50% Py 25 µm	8.50	4.95	1.28	0.743
50% Sp 825 µm	0.00	0.00	0.00	0.00
50% Sp 25 µm	0.00	0.00	0.00	0.00
50% Py + 50% Sp 825 µm	0.00	5.50	0.00	0.825
50% Py + 50% Sp @ 340 µm	0.70	0.70	0.105	0.105
50% Py + 50% Sp @ 70 µm	54.7	62.6	8.21	9.39
50% Py + 50% Sp @ 25 µm	180	142	27.0	21.2
50% Py (825 µm) + 50% Sp (25 µm)	5.80	8.40	0.87	1.26
50% Py (25 µm) + 50% Sp (825 µm)	42.3	57.7	6.35	8.66

Table A 5: Surface area for Py-Sp controlled particle size system, SHRs and SHCs

Surface Area with respect to; (m^2/g)			SHR (°C/hr)		SHC (J/g)	
Py	**Sp**	**Mean Py-Sp**	**A**	**B**	**A**	**B**
0.0199	0.6215	0.3207	0.00	5.50	0.00	0.825
0.1060	0.7165	0.4112	0.70	0.70	0.105	0.105
0.2243	0.9106	0.5675	54.7	62.6	8.21	9.39
0.4645	1.4550	0.9598	180	142	27.0	21.23